First publ. in: Journal of Chemical Physics 106 (1997), 1, pp. 347-375

Mode-coupling theory of the slow dynamics of polymeric liquids: Fractal macromolecular architectures

Matthias Fuchs and Kenneth S. Schweizer
Departments of Materials Science and Engineering and Chemistry, University of Illinois, 1304 West Green Street, Urbana, Illinois 61801

(Received 16 May 1996; accepted 25 September 1996)

Recently a mode coupling theory for the dynamics of solutions and melts of entangled linear chain polymers has been developed. We report the extension of this approach to macromolecular architectures different from linear chains. Specifically, this work addresses recent experimental findings on melts of ring shaped polymers, small spherical micro-networks, and linear chains in two dimensions. The mechanical and dielectric response, diffusion, and molecular relaxation times of macromolecules modeled by fractal mass distributions are studied. The distribution is chosen to be Gaussian and then is uniquely determined from the experimentally measured scaling of macromolecular size (R_g) with degree of polymerization (N), i.e., $R_g \propto N^{\nu}$. The exponent ν and the spatial dimension d determine the large N scaling of the transport coefficients and the exponents describing intermediate time anomalous diffusion. Within the theory, entanglement corrections to the single polymer Rouse dynamics are effective for $\nu < 2/d$ only. There, we find $D \propto N^{2d\nu-5}$ for the diffusion coefficient and that the ratio $D\tau_D/R_g^2$ is almost constant, where τ_D is the terminal relaxation time. Using independent input from equilibrium liquid state theories, the magnitude and scaling with macromolecular density and segment length of the dynamical properties is determined. It is also found that macromolecular interpenetration requires progressively higher densities and consequently entanglements become less effective with fractal dimension $1/\nu$ approaching the spatial dimension.

I. INTRODUCTION

The dynamics of dense polymer liquids has attracted interest for a long time.[1] Chain molecules consisting of many repeat units, monomers, have been studied because of their technological importance and intrinsic interest. Systems of chain polymers with a large degree of polymerization exhibit very slow dynamical processes connected to the so-called ''entanglements,'' which are viewed as a consequence of chain connectivity and excluded volume intermolecular interactions. Important progress has been achieved by an elegant phenomenological approach, the reptation or tube model, which is amply discussed in monographs.[2,3] It circumvents the problem to define entanglements, or to show how they arise within more microscopic descriptions, by postulating their effects as constraints for the motion of a single probe polymer. This leads to a rather concrete picture of the long time anisotropic motion of a single chain polymer in a melt, it slides in a tube. The characteristic slow process of entangled polymers then is connected to the conformational relaxation triggered by the chain ends leaving the tube.[2,3] Numerous phenomenological extensions of this approach relax different aspects of the constraints in different ways, but still do not address the microscopic origin of entanglements or the fundamental validity of the tube ansatz.[4–6] Several alternative, non-reptation and/or non-tube phenomenological theories have also recently been proposed.[7–9] The semi-empirical cooperative cluster theory of Douglas and Hubbard[7] is of particular interest to our present work since it also addresses the role of macromolecular fractal and spatial dimensions on entanglement phenomena.

Recent progress in the synthesis of non-linear architectures has raised the possibility of studying the effects of macromolecular architecture on the entanglement problem. Melts of cyclic polymers,[10,11] star polymers,[12,13] H-shaped polymers,[14] comb-like polymers,[15] and of differently cross-linked micro-networks or micro-gels[16–18] have been prepared and studied for entanglement effects. In contrast to a naive interpretation of the reptation picture, it is found that macromolecules irrespective of their molecular architecture show a slow relaxation process above a certain crossover degree of polymerization. In several cases the observed phenomenology is remarkably similar to linear chain polymers. A number of phenomenological models have been advanced to explain some of these observations.[19–23] They share with the reptation model the aspect that the surrounding melt is viewed as imposing nearly static constraints, and that only specific, architecture-dependent idealized modes of motion are allowed for the probe. A number of experimental findings can be rationalized with these approaches but the phenomenon that entanglement effects show rather common features for different macromolecular architectures appears accidental. Let us mention one striking observation, namely, the plateau value in the shear modulus which is rather close for polystyrene molecules of different topologies (including spherical microgels), whereas for linear polymers of different chemical units larger variations are observed.[1,10–16] Of course, one has to caution that the impression that a slow dynamical entanglement process is a common feature of strongly interacting macromolecules may be premature as experiments may often be in a broad crossover region, where

different transport processes compete and simplified theoretical models do not yet apply. At present this question appears to preclude the possibility of experimentally verifying the original tube model for linear chains and $N\to\infty$, although it is well known that systematic deviations are observed.[1–3,6] Also, it is clear that the study of dynamic processes in cyclic polymers does not necessarily address the question ''do linear chains reptate,''[6] and it should be mentioned that recent microscopic theories have suggested approximations to connect the tube model parameters to equilibrium properties of the polymer melt.[24–26] However, the wealth of experimental studies suggests a more universal underlying mechanism for entanglement formation and relaxation in macromolecular liquids than implicitly assumed in most phenomenological models.[16]

Recently, one of us has put forward a new microscopic approach to the entanglement problem in melts,[27–32] which was extended to solutions,[33,34] blends[35,36] and copolymers.[37–39] It generalizes established techniques and approximations from theories for the equilibrium structure and dynamics of simple liquids, and addresses the question how the microscopic equations of motion containing the molecular potentials explicitly lead to entanglement effects. A unique feature of the theory is its suggestion of an underlying equilibrium structural origin of entanglement formation and slow relaxation in rough analogy with the phenomena of critical slowing down,[40] anomalous diffusion in fractal media,[41] and caging in simple and colloidal fluids.[42,43] As the theory uses no *a priori* assumptions about specific probe motions or constraints imposed by the surrounding melt, it naturally can be used to study various molecular architectures. The question whether the non-reptative, isotropic dynamics adopted by the theory is literally true for all polymeric architectures, especially linear chains, or is merely an adequate effective-medium-description remains unresolved.[32] The quantities which are input into the theory, in principle, can be measured and detailed questions about dependences on polymer density and chemical parameters may be addressed. The case of linear chain molecules has been discussed using asymptotic results for large degrees of polymerization,[27–31,33,34] and numerical solutions to the full equations in experimentally relevant parameter ranges including crossover effects.[31,32]

In this paper this microscopic approach is extended to fractal macromolecular architectures. The extension to nonlinear polymers is clearly motivated by the experiments quoted above, and the observed common features of the entanglement effects. Gaussian fractal macromolecules are considered because of the following reasons. First, the appropriate model of a single non-entangled fractal molecule has been studied by Cates and Muthukumar and serves as a reference point.[44,45] Second, linear polymers in melts and dense solutions are commonly described as Gaussian chains, i.e., as ideal random walks, which corresponds to a (mass-) fractal dimension of $d_F=2$. Gaussian fractal models appear the most simple variation to this known case, which is also relevant to experimental systems. Cyclic polymers in melts have been suggested to have a fractal dimension,[46–48] $d_F\approx 2.2$ to 5/2, and neutron scattering has demonstrated that some melts of the cross-linked micro-networks have a mass fractal dimension[17,18] $d_F\approx 3$. Third, as previous and this work show, the entanglement effects in the polymer mode coupling theory of Schweizer for chain molecules result from fluctuating force time correlations over a broad range of wave vectors where both the intramolecular structure and intermolecular packing correlations are self-similar.[30] The generalization to other fractal dimensions therefore appears naturally, and a few preliminary results have been published before largely without derivation.[30]

The dynamics of a single polymer with fractal dimension, d_F, which determines its size, $R_g\sim N^{1/d_F}$, has been studied for different interactions.[44,45] As polymers often are discussed in the context of critical phenomena[2] we will use this notation and define the size-mass scaling exponent ν, $\nu=1/d_F$. Cates and Muthukumar show that in the unentangled Rouse model, where hydrodynamic interactions are neglected, dynamical scaling[40] holds. The static scaling and the exponent ν is put into the fractal model by hand. Dynamical scaling entails the existence of a single, characteristic long time scale, τ^{R}, which scales like: $\tau^{\mathrm{R}}(N)\propto N^{z\nu}$. The dynamical exponent z is determined by noting that the longest relaxation time of the Rouse model corresponds to diffusion a distance of order the size of the macromolecule, $1/\tau^{\mathrm{R}}(N)\sim D^{\mathrm{R}}/R_g^2$ and that the diffusion coefficient is obtained from adding up N independent monomer friction forces, $D^{\mathrm{R}}=k_BT/\zeta_0 N$, where $\zeta_0=\zeta_{\mathrm{total}}/N$ is the ''bare'' local friction constant. The relation $z=2+1/\nu$ is found and reported in terms of the spectral fractal dimension,[44,45] $d_s=2/z\nu$. The static viscosity follows from a dumbbell consideration,[2] $\eta\sim(1/N)\,\zeta_{\mathrm{total}}R_g^2\sim N^{2\nu}$, and generalizes to finite frequencies ω by a simple scaling law, $\eta(\omega)=N^{2\nu}f_\eta(\omega\tau^{\mathrm{R}})$. This underlying simplicity in the dynamics of the non-interacting fractal macromolecules is another aspect motivating our study. It connects the entanglement problem to a class of models where the standard static and dynamic scaling results are well understood.

Deriving from first principles the dynamics of dense liquids of strongly interacting macromolecules necessarily requires approximations, some of which are not well controlled in the present theory. In order to highlight the contents of the theory let us list the central assumptions. (i) The crossover to entangled dynamics is described by the ''renormalized Rouse'' (RR) theory which, for linear chains, is discussed in Refs. 27 and 33. (ii) The slow dynamics of entangled polymers is described by the ''polymer mode coupling'' (PMC) theory which is discussed in Refs. 27, 28 and 32. (iii) It is argued that chain-end effects (or more generally static and dynamic site inequivalency) and the exact treatment of the low lying modes do not affect the presented results. We argue that these simplifications are not important for architectures such as linear chains, rings, and (perhaps) spherical microgels, systems for which our predictions seem to be in good accord with experiments. However, these simplifications are not appropriate for other topologies such as stars, some types of branched polymers, and rigid rods. For example, the nearly exponential dependence of star melt vis-

cosity and diffusion constant on arm molecular weight predicted by phenomenological arm retraction ideas within the tube model,[2,3,49] and found in many (but not all) experiments,[16,50–52] is not predicted. A very large enhancement of the rotational relaxation time and shear viscosity of isotropic rigid rod solutions[53–55] is also not captured. (iv) Only well-defined single molecule correlation functions are calculated. Some experimental quantities are assumed to be dominated by the single molecule contribution, e.g., the shear stress. (v) A special class of polymer topologies is studied. Only macromolecules whose intramolecular structure is experimentally found to be described or approximated by a Gaussian fractal model are studied. Limitations of this restriction are mentioned in point (iii) above. (vi) The information about the equilibrium liquid structure, which is required as an input to the dynamical theory, is calculated within an integral equation approach. In principle experiment or simulation could provide more accurate information replacing this calculation. (vii) Polymeric solutions are treated as effective, lower density one-component systems. Hydrodynamic interactions, and corrections to the Gaussian intramolecular structure (with the exception of a density-dependent effective statistical segment size), are neglected. (viii) Entanglement effects are turned off on length scales smaller than the crossover length calculated within the RR theory. A naive additive crossover description is used for finite molecular weights.

It is important to realize that although our theory has the above simplifications and limitations, it represents a novel attempt to develop a microscopic theory for the fluctuating force time correlations and friction within a general framework which can simultaneously treat (some) different macromolecular architectures. This feature is in strong contrast with phenomenological approaches such as the tube model which are based on rather specific guesses for the dominant disentanglement stochastic trajectories which are modified for different architectures. Moreover, a variety of experimentally accessible quantities are predicted and allow cross-checks of the underlying physical picture and the theory.

Although, the full time dependence of the mean squared displacements (center-of-mass and segmental), shear stress and dielectric relaxation, and single polymer density fluctuations are predicted, the most easily tested predictions probably concern the transport coefficients for different fractal dimensions. We find that the entanglements in the theory arise from two-molecule binary monomeric contacts, which matter for geometric reasons for $\nu<2/d$ only. Reservations are required when applying this result to rigid rods where specific topological interactions exist. Based on our theory of equilibrium liquid structure, we find (in agreement with experiments and simulations[56,57]) in two and three dimensions that for dense fractal objects, i.e., for $d_F\rightarrow d$, interpenetration and consequently entanglement effects become unimportant for realistic polymer densities. Even when strong entanglement effects are operative, the theory predicts a competition between two trends with increasing fractal dimension: The enhanced exponent in the N-scaling of the number of two macromolecule contacts (proportional to $N^{2-d\nu}$) which increases friction, versus a reduction of the local contact value of the intermolecular site-site pair correlation function $[g_d=g(r=D)]$ which reduces friction. This aspect of the theory leads to qualitative agreement with experimental observations on entangled chain, ring, and microgel melts[10,11,16,58,59] which find that the magnitude of the shear viscosities are roughly macromolecular architecture independent in an intermediate crossover molecular weight region.[16] The theory predicts a similar behavior for self-diffusion constants. Experimental diffusion studies are roughly compatible with this prediction, although the former are still affected by the constraint release mechanism[60] which we have ignored for simplicity. In the pre-terminal, non-Markovian regime, our theory predicts power law frequency scaling of the disentanglement process as reflected in several loss modulii (e.g., stress and dielectric). An exponent of roughly 0.2 for the shear stress loss modulus, $G''(\omega)\sim\omega^{-0.2}$, is found for a range of experimentally relevant fractal dimensions. This exponent is in close agreement with chain experiments[58,59] and is much smaller than the asymptotic reptation/tube prediction of 1/2.

The contents of this manuscript is organized as follows. Section II collects the starting generalized Langevin equations of the theory. It is shown which experimentally measurable correlation functions can be calculated in this approach. Section III defines the fractal macromolecular model and obtains the equilibrium intramolecular information which are needed for the dynamical theory. In Section IV the collective fluid structure is analyzed using an integral equation approach. The input of the intra- and inter-molecular equilibrium structure is used in Section V to work out the dynamics of entangled fractal macromolecular fluids. Dependences of dynamical properties on time, frequency, fractal and spatial dimensionalities, degree of polymerization, polymer density, solvent quality and some coarse-grained chemical features are discussed. A comparison with the reptation/tube approach to fractal macromolecules is made. Large N asymptotic results are obtained analytically and a simplified crossover model is studied to estimate finite N effects in the range of experimentally relevant degrees of polymerization. Some connections to various experimental findings are discussed. The Appendix treats the case of fractal, rod-like macromolecules which are of intrinsic interest, and whose study sheds light on the neglect of chain end effects, low lying modes, and the origin of entanglement effects for the other fractal dimensions.

II. BASIC EQUATIONS

A. Segment position correlators

Recently, Schweizer has derived a set of linear, non-Markovian generalized Langevin equations for a tagged polymer chain molecule in a polymer solution or melt.[27–34] We will only summarize the final set of equations. For macromolecules of non-linear architecture only slight adjustments in the basic equations are necessary. The tagged molecule of N segments of statistical segment length, σ, experiences intra- and intermolecular forces. Following stan-

dard practice, the intra-molecular forces are approximated by the bead-spring or Rouse model.[3] New and non-trivial expressions have been suggested for the intermolecular forces, which the probe molecule feels when moving in a matrix of other polymers. Finally, equations of motion for the matrix of correlation functions $\langle \vec{R}_\alpha(t)\cdot\vec{R}_\beta\rangle$ are obtained, where $\vec{R}_\alpha(t)$ is the position vector of the segment or monomer α of the probe, $1\leqslant\alpha\leqslant N$. Using the following convention for the Laplace transform: $f(z)=\mathrm{LT}[f(t)](z)=i\int_0^\infty dt\ e^{izt}f(t)$, and matrix notation,[61] the system of equations are given by[27]

$$[z1+[1-im(z)]^{-1}i\overline{\Gamma}]\langle R(z)\cdot R^T\rangle=-\langle R\cdot R^T\rangle, \tag{1a}$$

$$m_{\alpha\beta}(t)=\frac{\beta}{d\zeta_0}\langle \vec{F}^Q_\alpha(t)\cdot\vec{F}_\beta(0)\rangle. \tag{1b}$$

Here, the intermolecular forces, $\vec{F}^Q_\alpha=-(\partial/\partial\vec{R}_\alpha)\times V(\{R\})$, depend on time via a projected dynamics partially decoupled from the slow dynamics. ζ_0 is the monomeric friction coefficient and $\beta=1/k_BT$. $\overline{\Gamma}_{\alpha\beta}$ denotes the initial decay rate associated with the bare, segmental scale dynamics,

$$\overline{\Gamma}=\langle R\cdot LR^T\rangle\langle R\cdot R^T\rangle^{-1}=dD_0\langle R\cdot R^T\rangle^{-1}, \tag{1c}$$

where the second equality follows from the absence of hydrodynamic interactions in the case of a d-dimensional melt. The Rouse model of course only considers $\overline{\Gamma}$ and assumes a vanishing memory function, $m_{\alpha\beta}(t)=0$. The monomeric diffusion coefficient $D_0=k_BT/\zeta_0$ sets the microscopic time scale τ_0, $\tau_0=(\sigma^2/dD_0)$, and is assumed to be known from experiment. The intermolecular excluded volume force, $\vec{F}_\alpha(t)$, exerted on the probe segment α by all the other (matrix) polymers in the system are approximated in two different models.

In the renormalized Rouse model (RR) a (dynamical) weak coupling factorization of the four-point correlation function, Eq. (1b), results in[27]

$$\Lambda(z)=\frac{1}{N}\sum_{\alpha\beta}^{N} m^{(\mathrm{RR})}_{\alpha\beta}(z)$$

$$=\psi(\sigma^{d+2}/\tau_0)\int_0^\infty dk k^{d+1}\omega_k\frac{-1}{z+\dfrac{iD_0k^2}{\omega_k}}, \tag{2a}$$

where the memory function describes the isotropic drag the probe feels from the surrounding melt in a perturbative or short time fashion. The relaxation of the friction forces is governed by the diffusive dynamics of the probe, which is approximated to be the free, Rouse motion. As only the uniform contribution of the RR friction is required in the following we will study the simplified RR model replacing $m^{(\mathrm{RR})}_{\alpha\beta}(z)$ by $\delta_{\alpha\beta}\Lambda(z)$. This simplification does not affect the present work. The full RR model is studied in Refs. 27 and 33. The coupling parameter ψ,

$$\psi=\psi_0^{(d)}\varrho_m D^d(D/\sigma)^d g_d^2 S_0, \tag{2b}$$

with

$$\psi_0^{(d)}=\left(\frac{2\pi^{d/2}}{\Gamma(d/2)}\right)^3\frac{1}{d^4(2\pi)^d},$$

is a measure of the direct pairwise interactions or collisions the probe segments experience with the surrounding matrix monomers. The contact value, $g_d=g(D)$, of the intermolecular segment–segment pair correlation function, $g(r)$, at the effective segment hard core diameter D enters, as does the small wave vector value of the collective liquid structure factor, S_0, which is connected to the bulk compressibility, $S_0=\varrho_m k_BT\chi_T$, at monomer density ϱ_m. The numerical prefactors arise from angle integrals in d- dimensions; Γ denotes the gamma function. Physically, the parameter ψ is proportional to the mean square repulsive force on the segmental scale exerted on the tagged polymer by its surroundings. The wave vector integral in Eq. (2a) can be interpreted as a summation over the contributions to the fluctuating force correlations arising from dynamically correlated processes on length scale $2\pi/k$. The relevant spatial range of such melt-probe dynamic correlations in Eq. (2a) is specified by the tagged molecule static structure factor, ω_k, which is defined by the sum over all elements of the matrix of segment–segment equilibrium correlations, $\omega_{\alpha\beta}(q)=\langle e^{i\vec{q}(\vec{R}_\alpha-\vec{R}_\beta)}\rangle$

$$\omega_q=\frac{1}{N}\sum_{\alpha,\beta=1}^{N}\omega_{\alpha\beta}(q)=\frac{1}{N}\sum_{\alpha,\beta=1}^{N}\langle e^{i\vec{q}(\vec{R}_\alpha-\vec{R}_\beta)}\rangle. \tag{3}$$

Whereas the RR model is supposed to describe the onset of entanglements for small macromolecules, or entangled dynamics of long chains at short times, for longer times, where strong slowing down occurs, the intermolecular forces are approximated differently. In the polymer mode coupling model (PMC) the fluctuating forces are projected onto the N bilinear products of a probe segment and the collective matrix density fields. The resulting memory function is expressed as[27,28]

$$m^{(\mathrm{PMC})}_{\alpha\beta}(z)=\psi'(\sigma^{d+2}/\tau_0)\int_0^\infty dk\ k^{d+1}\omega_k^2\omega^{-1}_{\alpha\beta}(k)$$

$$\times\frac{-1}{z+\dfrac{iD_0k^2/\omega_k}{1-i\Lambda(z)}}, \tag{4a}$$

where $\Lambda(z)$ is the frequency dependent friction function of the RR model. The presence of the inverse of the static correlation matrix, $\omega_{\alpha\beta}$, accounts for the influence of macromolecular connectivity on the fluctuating, time dependent intermolecular force correlations. The projected dynamics of the PMC friction forces is evaluated from the RR model. The physical motivation for Eq. (4) has been extensively discussed.[27,28,32] An important feature of Eq. (4) is the spatially non-homogeneous friction captured in the explicit dependence of $m^{(\mathrm{PMC})}_{\alpha\beta}(t)$ on the monomer sites, α, β. Equally important is the diffusion pole of the RR dynamics determining the relaxation of the friction forces in Eq. (4a). In the coupling strength parameter, ψ', of the PMC model

$$\psi'=\psi'^{(d)}_0\varrho_m c_0^2 S_0/\sigma^d,\quad \text{with}\quad \psi'^{(d)}_0=\frac{2\pi^{d/2}}{\Gamma(d/2)(2\pi)^d d^2}, \tag{4b}$$

the direct hard sphere interaction captured in g_d of Eq. (2b) is replaced by the effective repulsive pseudopotential described by the direct correlation function at zero wave vector,[27] $c_0<0$. It has been argued that the PMC-friction function, when its dynamics is evaluated using the RR model, describes the long time dynamics of entangled polymers.[27,28,32] However, as has been discussed elsewhere,[31,32] the PMC model also affects the dynamics on very local length and time scales. This effect should be considered unphysical. In order to *quantitatively* compare to experimental studies the collective dynamical processes described by the PMC friction should be absent at short times and/or distances,[31,32] or only *long enough* length or time scales should be considered. Our present approach is in the latter spirit which also has the advantage of allowing analytical analysis in the large N limit. Interesting long time dynamics results from these models, Eqs. (2a) and (4a), as the friction functions pick up molecular weight or N-dependences due to the small wave vector structure in the integrands. Akin to the long time tails familiar from simple liquids,[62] anomalous diffusion arises in intermediate time windows. New N-dependent time scales arise from the variation of the molecular structure, ω_k, on the size of the probe molecule, R_g. This effect clearly bears similarity to dynamical critical phenomena, an aspect which also motivates our considerations of non-chain-like, fractal polymer architectures and general spatial dimensions.

Equations (1)–(4) determine the dynamics of the tagged macromolecule from its equilibrium structure as expressed primarily in terms of the matrix of partial structure factors, $\omega_{\alpha\beta}(q)$. Non-universal collective equilibrium structure and intermolecular packing only enters via the coupling parameters ψ and ψ'. Implicit in this simplification is the assumption that on the length scales of interest the equilibrium structure is homogeneous, e.g., $S_k \approx S_0$. Although valid as $N\to\infty$, significant finite size corrections can occur as discussed elsewhere.[31,32] A dynamically frozen matrix assumption has also been invoked corresponding to the physical assumption that the relaxation of the entanglement friction forces exerted on the probe is solely determined by the tagged particle dynamics via its *coherent* density fluctuations. We expect this simplification to be qualitatively reliable if the matrix is composed of polymers of degree of polymerization comparable to, or greater than, the probe N. These equations have been rather successfully applied to chain polymers in melt, blend, and copolymer environments.[31,32,35–39] In this paper we want to study the role of varying macromolecular architecture as captured in the static structure factors $\omega_{\alpha\beta}(q)$.

B. Observables

In this section we will connect various measurable quantities with the tagged polymer dynamics as described in the previous section. From the matrix of segment position correlators one can immediately obtain the probe averaged mean squared displacement, $\phi(t)$, by taking the trace

$$\phi(t)=\frac{1}{N}\sum_{\alpha=1}^{N}\langle(\vec{R}_\alpha(t)-\vec{R}_\alpha(0))^2\rangle, \tag{5a}$$

$$\phi(z)=-\frac{2dD_0}{Nz}Tr\{[\overline{\Gamma}-iz(1-im(z))]^{-1}\}. \tag{5b}$$

The center-of-mass motion, $\Phi(t)$, is obtained from $\langle R(t)\cdot R^T\rangle$ by projecting onto the normalized, N-dimensional vector of uniform translation, $V_{\rm CM}^T=(1/\sqrt{N})\,(1,\ldots,1)$

$$\Phi(t)=\langle(\vec{R}^{\rm CM}(t)-\vec{R}^{CM}(0))^2\rangle, \quad \text{where}$$

$$\vec{R}^{\rm CM}=\frac{1}{N}\sum_{\alpha=1}^{N}\vec{R}_\alpha, \tag{6a}$$

$$\Phi(z)=-\frac{2dD_0}{Nz}V_{\rm CM}^T[\overline{\Gamma}-iz(1-im(z))]^{-1}V_{\rm CM}. \tag{6b}$$

Without additional assumptions, which will be discussed in the next section, Eq. (6b) cannot be simplified further, since $V_{\rm CM}$ will in general not be an eigenvector of the friction matrix $m_{\alpha\beta}$.

We follow the standard assumption that the collective shear stress is dominated by the single molecule contribution arising solely from the elastic intra-molecular forces[3,28]

$$G(t)=\frac{\varrho_m}{k_BTN}\sum_{\alpha,\beta=1}^{N}\langle R_\alpha^x(t)f_\alpha^{\rm intra,y}(t)R_\beta^x(0)f_\beta^{\rm intra,y}(0)\rangle. \tag{7a}$$

Then, because of the linear equations of motion, Eq. (1), and spatial isotropy, a Rouse-like formula for the shear modulus, $G(t)$, is obtained[28]

$$G(t)=\frac{\varrho_m k_BT}{N}Tr\{\Gamma\langle R(t)\cdot R^T\rangle\Gamma\langle R(t)\cdot R^T\rangle\}/(dD_0)^2. \tag{7b}$$

Here, $\Gamma=Q_{\rm CM}\overline{\Gamma}Q_{\rm CM}$ is obtained from the inverse of the static correlations, Eq. (1b), by projecting perpendicular to the center-of-mass dynamics, $Q_{\rm CM}=1-P_{\rm CM}=1-V_{\rm CM}V_{\rm CM}^T$, thereby demonstrating that the intra-molecular stress is unaffected by the center-of-mass motion.

Closely related to the modulus is the segment elastic force correlation function which for chain molecules equals the bond vector autocorrelation function $(1/N)\Sigma_\alpha\langle\vec{b}_\alpha(t)\cdot\vec{b}_\alpha\rangle$, where[3] $\vec{b}_\alpha=\vec{R}_{\alpha+1}-\vec{R}_\alpha$

$$B(t)=\frac{1}{dk_BT}\frac{1}{N}\sum_{\alpha=1}^{N}\langle\vec{R}_\alpha(t)\cdot\vec{f}_\alpha^{\rm intra}(0)\rangle$$

$$=\frac{1}{N}Tr\{\Gamma\langle R(t)\cdot R^T\rangle\}/(dD_0). \tag{8}$$

Another quantity of interest is the radius of gyration fluctuation function, $P(t)$, which we will consider as a molecular architecture independent analog of the linear chain end-to-end vector correlation function

$$P(t)=\frac{1}{N}\sum_{\alpha=1}^{N}\langle(\vec{R}_\alpha(t)-\vec{R}^{CM}(t))\cdot(\vec{R}_\alpha(0)-\vec{R}^{CM}(0))\rangle$$

$$=\frac{1}{N}Tr\{Q_{\rm CM}\langle R(t)\cdot R^T(0)\rangle Q_{\rm CM}\}. \tag{9}$$

We follow the general assumption that the end-to-end vector fluctuations of certain linear chain polymers made up of dipolar monomers can be measured by dielectric spectroscopy,[63] and for general architectures discuss the dynamical radius of gyration correlation function, $P(t)$, with respect to dielectric measurements.

Whereas the linear equations of motion, Eq. (1), without further assumption lead to the Eqs. (5)–(9) for the mean squared displacements, the (single molecule) shear modulus, and the radius of gyration fluctuations, we tentatively also calculate correlation functions which are non-linear in the monomer positions. Using the Gaussian approximation and neglecting boundary effects the incoherent dynamic structure factor is connected to the averaged mean square displacement, Eq. (5) as

$$\omega^{\mathrm{inc}}(t,q)=\frac{1}{N}\sum_{\alpha=1}^{N}\left\langle e^{i\vec{q}(\vec{R}_\alpha(t)-\vec{R}_\alpha(0))}\right\rangle\approx e^{-(q^2/2d)\,\phi(t)}. \quad (10)$$

It can be measured by pulsed field gradient NMR.[64] The same Gaussian approximation also simplifies the single molecule coherent dynamic structure factor to

$$\omega^{\mathrm{coh}}(t,q)=\frac{1}{N}\sum_{\alpha,\beta=1}^{N}\left\langle e^{i\vec{q}(\vec{R}_\alpha(t)-\vec{R}_\beta(0))}\right\rangle$$

$$\approx\frac{1}{N}\sum_{\alpha,\beta=1}^{N}e^{-\frac{q^2}{2d}\langle(\vec{R}_\alpha(t)-\vec{R}_\beta(0))^2\rangle}. \quad (11)$$

It can be argued that the Gaussian approximation holds at very short times and in the long time, Markovian limit of Eq. (1). For intermediate times, however, its validity is doubtful.[27,32]

III. GAUSSIAN FRACTAL MODELS

A. Structure

Equations (1)–(4) directly relate the probe polymer dynamics and macromolecular and liquid equilibrium structure. The latter only enters via the system-specific parameters ψ and ψ' characterizing the strength of the fluctuating forces. The long range intra-molecular correlations, however, affect the dynamics differently on different length scales and lead to a sensitive dependence of the motion on polymer architecture. Although the linear, ideal chain molecule is the most experimentally relevant case other polymer architectures also invite study for several reasons. First, advances in chemical synthesis have introduced new non-linear macromolecules such as rings, stars, micro-networks or micro-gels.[10–18] Second, comparing the results for other architectures with the chain case may shed light on the transport mechanisms captured in the RR and PMC models. Third, due to the connections of our approach to the description of long time tails and critical slowing down, a study of models where the more universal large length scale properties are varied seems especially fruitful.[30] Therefore, we will focus on macromolecules where the radius of gyration, R_g, depends on mass, M, or monomer number, N, in a fractal way. A fractal (mass) dimension d_F, or its inverse, the exponent ν, $\nu=1/d_F$, is globally defined as

$$R_g\propto N^{\nu}, \quad \text{where} \quad \nu=1/d_F. \quad (12a)$$

Besides the case of random walk linear chains, where $\nu=1/2$, the following fractal objects are of experimental interest: Rod-like molecules,[3] where $\nu=1$, fractal micro-networks (or micro-gels),[17,18] and models for partially collapsed ring molecules in the melt, for which the dimension $d_F\approx 5/2$ has been suggested theoretically[46] and values ranging from $d_F\approx 2.22$ to $d_F\approx 2.56$ have been found in lattice simulations.[47,48] There are also melts composed of macromolecules with fractal dimension equal to the spatial dimension, as, for example, ideal random walk chains[56,57] in spatial dimension $d=2$, or fractal micro-networks in $d=3$ dimensions.[18] These structures differ from dense solid objects, which do not show fractal but Porod like scattering, $\omega_q\sim q^{-(1+d)}$, because they contain pores on all length scales and in principle allow interpenetration.

Real macromolecules clearly possess fractal structure only on length scales large compared to chemical or microscopic structural features. However, the detailed study of chain polymers[1–6,32] has shown that the description of the entanglement problem in Eqs. (1)–(4) is qualitatively insensitive to microscopic details on the 5-10 Angstrom scale. Assuming that this holds for different fractal objects as well, the simplest approach to extend the fractal mass-size scaling of Eq. (12a) to describe the structure of the macromolecule on all length scales is to postulate that the spatial distance of two monomers α, β is connected to their chemical distance by the same exponent ν

$$\langle(\vec{R}_\alpha-\vec{R}_\beta)^2\rangle=\sigma^2|\alpha-\beta|^{2\nu} \quad \text{for} \quad 1\leqslant\alpha,\beta\leqslant N. \quad (12b)$$

Some unspecified labeling scheme is assumed to determine the chemical distances; it will of course depend on molecular architecture, e.g., connectivity. In the present form of the PMC approach, however, the results are determined by the mass structure only, independent of the underlying connectivities which are the origin of a particular mass distribution. Assumption Eq. (12b) therefore is the simplest extension of the global scaling law, Eq. (12a), introducing no new physical effects down to the monomeric size, σ. Let us emphasize that Eq. (12b) excludes the study of some interesting polymeric architectures. Semi-flexible chains are characterized by a further length scale, the persistence length, which can be large compared to monomeric sizes. In the present treatment semi-flexible chains are contained only if all dynamical entanglement effects arise at distances large compared to the persistence length, which then can be viewed as the size of an effective segment. Also star polymers can be described with Eq. (12b) in frequency windows only where the dynamical effects arise from the Gaussian-chain-like arms of the star. The segments of a star are not all equivalent. The global topological difference of a star and a chain polymer clearly cannot be captured by a fractal polymer model. However, it must be pointed out that dielectric,[51] viscoelastic[16] and diffusion[52] measurements all have shown that there is an

intermediate region of dynamical behavior (roughly $N_e < N < 4-6N_e$) where stars show entanglement features very similar to linear chains, e.g., power law growth with N of relaxation times as opposed to exponential growth. For this intermediate regime we expect our theoretical approach is useful.

An expression for the matrix of intramolecular structure factors, $\omega_{\alpha\beta}(q)$, is needed. A Gaussian model is consistent with the assumption of elastic intramolecular forces in Eq. (1), $\vec{f}_\alpha^{\,\mathrm{intra}} \propto \Sigma_\beta \Gamma_{\alpha\beta} \vec{R}_\beta$, and leads to

$$\omega_{\alpha\beta}(q) = e^{-\frac{q^2}{2d}\langle(\vec{R}_\alpha - \vec{R}_\beta)^2\rangle}. \tag{12c}$$

From Eqs. (3), (12b), and (12c) the intramolecular structure factor ω_q and its asymptotic expressions can be found

$$\omega_q \rightarrow \begin{cases} N(1-q^2R_g^2/d) & qR_g \ll 1, \quad \text{where } R_g^2 = \dfrac{N^{2\nu}\sigma^2}{(2\nu+1)(2\nu+2)} \\ (q\sigma\sqrt{c_1})^{-1/\nu} & 1/R_g \ll q \ll 1/\sigma, \quad \text{where } c_1 = \dfrac{1}{2d(2\Gamma(1+1/2\nu))^{2\nu}} \end{cases}. \tag{12d}$$

Neutron scattering experiments, in principle, can study the intramolecular structure factor, ω_q, determining the power law wave vector dependence in Eq. (12d) or the scaling of the radius of gyration, Eq. (12a). Therefore, the underlying fractal geometry can be revealed experimentally from measuring the scalar mass distribution. Our more detailed assumptions (12b) and (12c) can be viewed as a minimalistic model determining the necessary static input solely from the exponent ν measured in such a scattering experiment.

Even without a Gaussian assumption, the matrix of the mean squared displacements is simply connected to the small q limit of the matrix of intramolecular structure factors

$$\langle(\vec{R}_\alpha - \vec{R}_\beta)^2\rangle = -\lim_{q\to 0}(2d/q^2)\sum_{\gamma,\delta} Q^{\mathrm{CM}}_{\alpha\gamma}\omega_{\gamma\delta}(q)Q^{\mathrm{CM}}_{\delta\beta}. \tag{13a}$$

Therefore, specifying $\omega_{\alpha\beta}(q)$ fully determines the dynamical Eqs. (1)–(4). A slight technical adjustment is necessary because the equilibrium center-of-mass fluctuations cannot be specified. The matrix $\langle \vec{R}_\alpha \cdot \vec{R}_\beta \rangle$ is not well defined since its inverse, $\overline{\Gamma}$, has a single eigenvalue of zero. This arises as the sum of all intramolecular forces on one molecule vanishes, $\Sigma_\alpha \vec{f}^{\,\mathrm{intra}} = 0$. If the molecule is placed in an external potential of order ε, then the initial decay rate and its inverse are well defined[65]

$$\overline{\Gamma} = dD_0[(\sigma^2/\varepsilon)P^{\mathrm{CM}} + \lim_{q\to 0}(d/q^2)Q^{\mathrm{CM}}\omega(q)Q^{\mathrm{CM}}]^{-1}, \tag{13b}$$

and physical observables are calculated by taking $\varepsilon \to 0$ at the end. As the formalism detailed in the next section explicitly splits off the center-of-mass mode, taking the limit $\varepsilon \to 0$ is straightforward and will not be mentioned explicitly.

Of main interest are the effects of the long range fractal geometry. Only small quantitative errors will be introduced by using instead of the exact ω_q the standard interpolation[3] between the asymptotic limits

$$\omega_q = \frac{N}{(1 + c_1 q^2\sigma^2 N^{2\nu})^{1/2\nu}}. \tag{14}$$

This expression allows analytic evaluation of a number of integrals appearing in the theory. A normalized scaling form $\hat{\omega}(x)$ will be used repeatedly, where $\hat{\omega}(x) = \omega(x = q\sigma N^\nu)/N$ will be approximated from Eq. (14); of course, the correct $\hat{\omega}$ from Eqs. (10) and (12c) could enter in numerical evaluations.

B. Spectral densities

The equations of motion are determined from the above equilibrium considerations. In principle numerical solutions of the N coupled equations would require simultaneous diagonalization. Whereas in the Rouse and the simplified[27,33] RR models which assume uniform friction this procedure can be achieved by one orthogonal transformation, in the PMC problem simultaneous diagonalization of $\overline{\Gamma}_{\alpha\beta}$ and $\omega_{\alpha\beta}(q)$ is not rigorously possible. Even in the case of Gaussian chains the well known Rouse eigenmodes only diagonalize $\overline{\Gamma}_{\alpha\beta}$ but not $\omega_{\alpha\beta}(q)$. The complications, however, only arise because of the finite size of the molecule. If periodic boundary conditions could be assumed, plane waves, $\propto \exp[2\pi ip/N]$, would trivially diagonalize the problem. Such results hold in the general case of Toeplitz matrices, $m_{\alpha\beta}$, i.e., matrices which depend on the difference of the indices only, $m_{\alpha\beta} = m_{(\gamma)}$, where $\gamma = \alpha - \beta$. Although little is known about the exact eigenvalues of general Toeplitz matrices, it is well known that the distribution of eigenvalues can easily be found by Fourier transformation[66] in the limit of large N.

Let us recall the pertinent results and apply them to the N-dimensional Toeplitz matrix $\omega_{\alpha\beta}(q) = \omega^{(N)}_{(\gamma)}(q)$ from Eq. (12c). For finite wave vectors it is possible to define the density of eigenstates ω_q^λ via:

$$\omega_q^\lambda = \sum_{\gamma=-\infty}^{\infty} e^{i\lambda\gamma}\omega^{(\infty)}_{(\gamma)}(q) = \sum_{\gamma=-\infty}^{\infty} e^{i\lambda\gamma} e^{-\left(\frac{q^2\sigma^2}{2d}|\gamma|^{2\nu}\right)}. \tag{15a}$$

For any smooth function g of the N exact eigenvalues $\omega_p^{(N)}(q)$, where the label p runs between $p=(-N+1)/2,\ldots,(N-1)/2$ for odd N, we can use a theorem by Szegö. It states that for large N a sum over all eigenvalues may be replaced by an integral using the density of states[66]

$$\lim_{N\to\infty}\frac{1}{N}\sum_{p=-(N-1)/2}^{(N-1)/2} g(\omega_p^{(N)}(q))=\int_{-\pi}^{\pi}\frac{d\lambda}{2\pi}g(\omega_q^{\lambda}). \tag{15b}$$

Of course, ω^{λ} is just a one-dimensional density of states well known from solid state theories. For large N each element of the matrix $\omega_{\alpha\beta}$ converges to a limit as if periodic boundary conditions applied[66]

$$\omega_{\alpha\beta}^{(N)}(q)\to\frac{1}{N}\sum_{p=-(N-1)/2}^{(N-1)/2} e^{-i\frac{2\pi p}{N}(\alpha-\beta)}\omega_q^{2\pi p/N} \quad \text{for } N\to\infty. \tag{15c}$$

This result can be interpreted as if the eigenvalues converged to the values $\omega_q^{\lambda_p^{(N)}}$ where the Fourier variable λ is equally spaced at $\lambda_p^{(N)}=(2\pi p)/(N)$ and $p=(-N+1)/2,\ldots,(N-1)/2$. However, it must be stressed[66] that Eq. (15c) only holds in the sense that the *distributions* of the exact eigenvalues and the $\lambda_p^{(N)}$ agree for large N.

From Eq. (13b) it can be seen that the eigenvalues of the initial decay, or Rouse rate, can be obtained from the exact eigenvalues $\omega_{\alpha\beta}^{(N)}(q)$ of the matrix $\omega_{\alpha\beta}$. $\overline{\Gamma}$ has a unique lowest eigenvalue, the center-of-mass eigenvalue $\overline{\Gamma^0}=\varepsilon$ (in the external potential) with eigenvector V_{CM}, and the $(N-1)$ further eigenvalues labeled by p

$$\Gamma^{\lambda_p^{(N)}}=dD_0/\left(\lim_{q\to 0}\frac{d}{q^2}\omega_q^{\lambda_p^{(N)}}\right), \tag{15d}$$

where

$$-\pi\leqslant\lambda_p^{(N)}\leqslant\pi,\lambda_p^{(N)}\neq 0\,.$$

In the case of random walk ideal chains, $\nu=1/2$, the corresponding formulae are known; the density of states of the intramolecular structure factors is[66]

$$\omega_q^{\lambda}=\frac{1-f^2}{1+f^2-2f\cos(\lambda)} \quad \text{for } \nu=1/2,$$

where

$$f=e^{-(q\sigma)^2/2d}.$$

The well known Rouse spectrum also follows because of Eq. (15d):

$$\Gamma^p=4(dD_0/\sigma^2)\sin^2(\tfrac{1}{2}\lambda_p^{(N)}) \quad \text{for } \nu=1/2.$$

Note, however, that the exact eigenvalues of Γ depend on the boundary considerations. For linear chains, $\lambda_p^{(N)}=(\pi p/N)$ for $0\leqslant p\leqslant N-1$ follows from the exact eigenvalue conditions. For ideal Gaussian rings with periodic boundary conditions, $\lambda_p^{(N)}=(2\pi p/N)$, for $(-N+1)/2\leqslant p\leqslant(N-1)/2$, is obtained leading to doubly degenerate eigenvalues. The lowest finite eigenvalue differs by a factor of 4 for the two boundary conditions. Moreover, the appropriate eigenvectors differ, as they will do in general, so that physical questions such as the translational-rotational coupling, which will enter Eq. (1) because of the memory functions, require additional considerations.

The approach put forward by one of us[27,28] when considering the entanglement problem of chain polymers focuses on the slowing down of internal modes neglecting chain end effects. In this paper we will extend this approach to macromolecules with fractal distributions of internal modes and neglect the question of the exact position of the lowest lying modes and the appropriate boundary conditions. Justifying this approach, the entanglement effects in Eqs. (1)–(4) will mostly result from considerations where the spectrum of internal modes dominate. They will be affected very little by an arbitrary cut-off factor $\lambda_c=(x\pi/N)$ which we introduce into the spectrum to keep track of the effects of this approximation. This approximation of course was also implicit in the studies of the Rouse problem for fractal polymers.[44,45] It may be called one of the defining physical assumptions which allows one to extend the approach put forward in Refs. 27 and 28 to different architectures without specifying the detailed real space transport mechanism as is necessary in reptation-tube based approaches.

The diagonalization of the Rouse and the simplified RR model, where only the matrix structure of the initial rate enters, is straightforward and results in the renormalized Rouse propagator, $C_{\lambda}^{(\mathrm{RR})}(t)$, normalized to unity at $t=0$

$$C_{\lambda}^{(\mathrm{RR})}(z)=\frac{-1}{z+\dfrac{i\Gamma^{\lambda}}{1-i\Lambda(z)}}. \tag{16}$$

As a first simplification in the PMC calculation it will be assumed that the center-of-mass motion decouples from the internal modes and Eq. (6b) becomes

$$\Phi(z)=\frac{2i}{N(-iz)^2}\frac{1}{1-i\Sigma(z)}, \tag{17a}$$

where the center-of-mass friction function is obtained from the uniform part of the PMC memory function and the large N approximation from Eq. (15c)

$$\Sigma(z)=V_{\mathrm{CM}}^T m(z)V_{\mathrm{CM}}=\psi'\int_0^{\infty}dk k^{d+1}\omega_k\frac{-1}{z+\dfrac{i(k^2/d\omega_k)}{1-i\Lambda(z)}}. \tag{17b}$$

In Eq. (17), and in the remainder of the paper, dimensionless units are used by rescaling $t\to t/\tau_0$, $q\to q\sigma$ and $R\to R/\sigma$. This expression for $\Sigma(z)$ can more directly be obtained from a mode coupling approximation by projecting the fluctuating forces onto the product of the matrix collective density and the coherent intramolecular density fluctuations, $\omega(q,t)$, see Refs. 27 and 36.

The internal modes are connected to the density of states of the intramolecular structure, ω_q^{λ}, which will be evaluated in the continuum description familiar from most polymer

theories,[3] i.e., the limit $N\to\infty$ and $q\sigma\to 0$ with $qR_g=$ fixed will be taken. The Fourier series results in Eqs. (15) then turn into the ones for Fourier transformations.

The averaged mean squared displacement of Eq. (5) then can be calculated in the PMC-model from

$$\phi(z)=\Phi(z)-(2/z)\int_{\lambda_c}^{\infty}\frac{d\lambda}{\pi}\,\frac{1}{\Gamma^{\lambda}-iz(1-im^{\lambda}(z))}, \qquad (18)$$

where the Fourier transformed friction function follows from Eq. (4a)

$$m^{\lambda}(z)=\psi'\int_0^{\infty}dk\,k^{d+1}(\omega_k^2/\omega_k^{\lambda})\frac{-1}{z+\dfrac{i(k^2/d\,\omega_k)}{1-i\Lambda(z)}}. \qquad (19)$$

It also determines the generalized, normalized Rouse propagator

$$C_{\lambda}^{(\mathrm{PMC})}(z)=\frac{-1}{z+\dfrac{i\Gamma^{\lambda}}{1-im^{\lambda}(z)}}, \qquad (20)$$

which enters into the stress modulus, Eq. (7),

$$G(t)=\varrho_m k_B T\int_{\lambda_c}^{(\pi/N_e)}\frac{d\lambda}{\pi}(C_{\lambda}^{(\mathrm{PMC})}(t))^2. \qquad (21)$$

The radius of gyration correlation function, $P(t)$ from Eq. (9), follows from the unnormalized generalized Rouse correlators

$$P(t)=\int_{\lambda_c}^{\infty}\frac{d\lambda}{\pi}C_{\lambda}^{(\mathrm{PMC})}(t)/\Gamma^{\lambda}. \qquad (22)$$

An upper mode cut-off has been introduced in Eq. (21). As is known from the work on the ideal random walk chain, the RR and PMC descriptions break down at short length and time scales where any theory should recover the bare Rouse dynamics. The correct crossover from unentangled local to the long time and large distance dynamics of Eqs. (1)–(4) has to be enforced by hand.[31,32] The cutoff at π/N_e enforces the physically sensible constraint that motions on the $\sqrt{N_e}$ and smaller scales remain Rouse-like and unaffected by the mode-coupling effects. In Section V D we will discuss the consequences of the higher modes, $\lambda>(\pi/N_e)$.

Whereas the incoherent, single monomer dynamic structure factor in the Gaussian approximation, Eq. (10), trivially follows from Eq. (18), the use of the spectrum ω_q^{λ} and the decoupling of the center-of-mass does not yet reduce the coherent, single molecule dynamic structure factor, $\omega^{\mathrm{coh}}(q,t)$, to a form which can be analyzed easily

$$\omega^{\mathrm{coh}}(q,t)=2\int_0^{N/2}d\gamma\,\exp\left\{-\frac{q^2}{2d}\left[\gamma^{2\nu}+\Phi(t)+2\int_{\lambda_c}^{\infty}\frac{d\lambda}{\pi}\,\frac{\cos(\lambda\gamma)}{\Gamma^{\lambda}}(1-C^{\lambda}(t))\right]\right\}. \qquad (23)$$

Here, the upper limit, $N/2$, in the integration was introduced by hand in order to correctly obtain the trivial sum rule $\omega^{\mathrm{coh}}(0,0)=N$.

Equations (16)–(23) are the dynamical equations which will be analyzed in the remainder of this paper. The structural information ω^{λ} needs to be calculated from the fractal model, Eq. (12). Only in the ideal coil case of $\nu=1/2$ and the rod-like case of $\nu=1$ can ω_q^{λ} be expressed by simple formulae

$$\omega_q^{\lambda}=\frac{q^2/d}{(q^2/2d)^2+\lambda^2}\quad\text{for}\quad\nu=1/2, \qquad (24a)$$

$$\omega_q^{\lambda}=\frac{\sqrt{2\pi d}}{q}e^{-(\lambda^2 d)/(2q^2)}\quad\text{for}\quad\nu=1, \qquad (24b)$$

In the general case, $\nu<1$, $\nu\neq 1/2$, ω_q^{λ} has a simple scaling form $\omega_q^{\lambda}=q^{-1/\nu}f^{\nu}(\lambda/q^{1/\nu})$ and exhibits the following asymptotes:[67]

$$\omega_q^{\lambda}\to\begin{cases}(q\sqrt{c_1})^{-1/\nu} & \text{for } \lambda\ll q^{1/\nu},\\ (q^2/\lambda^{1+2\nu})(c_2/d) & \text{for } \lambda\gg q^{1/\nu},\ c_2=\Gamma(1+2\nu)\sin(\pi\nu),\end{cases} \qquad (24c)$$

where c_1 is defined in Eq. (12d). In the first limit, the spatial resolution $1/q$ is within the cluster of $1/\lambda^{\nu}$ monomers and sees the fractal mass distribution. In the second limit, the factor q^2 indicates the negative scattering interference for the non-homogeneous mode λ. In the following, the inverse of ω_q^{λ} is also needed. Instead of using the full form, we will (as in the case of the macromolecular structure factor ω_q) replace it with the Pade-interpolation between the asymptotes

$$\omega_q^{\lambda}\approx\frac{q^2c_2}{c_2q^2(q\sqrt{c_1})^{1/\nu}+d\lambda^{1+2\nu}}. \qquad (24d)$$

This approximation is of similar quantitative accuracy as the approximation Eq. (14). It is consistent with the assumed statistical equivalence of all segments of the macromolecule. Topological corrections such as the cyclic nature of a ring polymer can be included but are ignored in the simple form above. Combining Eqs. (24d) and (19) leads to the possibility of separating the mode-dependent friction function in the PMC-model into two mode-index-independent memory functions $\Sigma'(z)$ and $M(z)$. The second one of these enters with a mode-dependent prefactor $\lambda^{1+2\nu}$. With the approximation Eq. (24d) we recover this result as first found by Schweizer in the study of Gaussian chain molecules,[28] where it is exact. From the second limit in Eqs. (24c) and (15d), the

initial decay, or Rouse rate, immediately follows for the fractal models for $\nu<1$

$$\Gamma^{\lambda}=\lambda^{1+2\nu}/c_2. \tag{25}$$

This spectrum of the elastic intra-molecular restoring forces is the one used by Cates and Muthukumar in their fractal Rouse models.[44,45] Let us recall the general result[66] that the exact eigenvalues $\Gamma_p^{(N)}$ generically depend quadratically on p for small p, $p \ll N$, for any fractal dimension, $\nu<1$. Only results which are determined by the broad range of intermediate modes can reliably be obtained from the fractal spectrum, Eq. (25), by setting $\lambda=(2\pi p)/(N)$.

In this section a series of well defined steps has led to the appearance of fractal dependences on wave vector q and Fourier variable λ. Ill-controlled technical approximations when simplifying Eqs. (1)–(4) were necessary both for the lowest lying eigenmodes as well as for the most microscopic ones. These approximations, however, are consistent with the approach leading to the starting Eqs. (1)–(4) as they describe a mechanism where the internal modes in an intermediate range dramatically slow down for large N. The employed fractal model architectures, including the ideal random walk, presuppose the relative unimportance of microscopic length scales. Experimentally this is supported by the finding that the dynamical length scale characterizing the entanglements is of intermediate size, typically $\sqrt{N_e}\sigma \approx$30-80 Å in the melt.[6] The neglect of rotational-translational coupling and the low-lying modes prevents studies of ''chain-end'' effects. However, the Appendix studies the case of Gaussian rod-like molecules where $d_F=\nu=1$. For this ν the approach seems to fail most spectacularly as the Rouse spectral density Γ^{λ} vanishes identically; see Eqs. (15d) and (24b). The formalism of this section correctly captures that for these Gaussian rod molecules, defined by $\omega_{\alpha\beta}(q)=f^{(\alpha-\beta)^2}$, where $f=\exp(-(q\sigma)^2/2d)$, the Rouse spectrum consists of two modes only: rigid rotation and center-of-mass translation.[65] In this case rotational-translational coupling can be studied explicitly and one finds that its effect on the RR and PMC approach is negligible. The present approach differs from reptation/tube based models in that it attributes no special role to the end segments but rather focuses on the slowing down of a growing number of self-similar internal modes.[3,28]

IV. LIQUID EQUILIBRIUM STRUCTURE

The equilibrium structure of the polymer liquid the probe is immersed in enters only via four parameters: monomer density ϱ_m, isothermal compressibility $\chi_T=S_0/(\varrho_m k_B T)$, contact value of the intermolecular segment-segment pair correlation function g_d, and the zero wave vector direct correlation function, c_0, which can be viewed as an effective repulsive pseudopotential. As collective structure functions of dense liquids and (simple) polymer melts are dominated by the excluded volume interaction, it is well justified to neglect wave vector dependences in the structure factor, S_q, or in c_q on the length scales $q\sigma \ll 1$ of interest in this work.[68] Clearly, the magnitude of the friction forces as described by the coupling parameters ψ, Eq. (2b), or ψ', Eq. (4b), will affect the relevance of entanglements for different architectures. Although within the framework of a coarse-grained Gaussian model one cannot hope to calculate ψ and ψ' quantitatively correctly, we do want to study their relative dependences on fluid density and the fractal dimensions of our model systems, Eq. (12). In this section we will use the polymer reference interaction site model (PRISM) of Curro and Schweizer[68,69] in order to estimate the trends in these parameters. Like the probe macromolecule the (identical) matrix polymers will be considered to have an internal structure described by ω_q of Eqs. (12) or (13). As the PMC or RR equations are determined by the relatively long wavelength aspects of the equilibrium structures, the most coarse-grained PRISM description, the analytic thread limit,[70] will be used. The precise values of ψ and ψ' will differ from results of more chemically realistic numerical PRISM calculations.[70] In the case of ideal Gaussian chain melts, previous studies[33] allow us to determine the ratio (A) of the ψ parameters evaluated within the thread and numerical calculations, similarly the ratio B for the ψ' parameter. The ratios A and B will be assumed to be independent of molecular architecture and polymer density. Therefore, the trend with fractal dimension and density can be obtained from the appealingly simple thread considerations.

PRISM theory is an extension of the RISM integral equation approach of Chandler and Andersen[62,71] for small molecule fluids to polymeric systems.[68,69] It determines the collective density structure factor, S_q, and the macromolecule averaged direct and indirect intermolecular site-site pair correlation functions, c_q and h_q, from the monomer density, ϱ_m, and from the intra-molecular structure as specified by ω_q. The defining equation for a one-component fluid composed of macromolecules with equivalent sites is

$$S_q=\omega_q+\varrho_m h_q=\omega_q/(1-\varrho_m c_q \omega_q). \tag{26}$$

As in the PMC or RR dynamical equations, chain end effects are not considered explicitly in Eq. (26). The excluded volume interaction is taken into account by requiring the site-site pair correlation function, $g(r)=1+h(r)$, to vanish inside an (effective) hard sphere diameter, D, characterizing the size of the basic chemical units or interaction sites of the polymer. The equations are closed by formulating approximate conditions on the direct correlation function, $c(r)$. For an extensive discussion of PRISM studies for different systems and varying microscopic details see Refs. 68 and 72.

In the thread limit[70] the effective hard sphere diameter D is shrunk to zero and the excluded volume constraint is enforced at the origin, $h(r=0)=-1$. Non-trivial solutions to Eq. (26) are assured by simultaneously taking the limit of an short range, infinite effective potential, $c(r)\to c_0\delta(r)$ in the spirit of the Percus-Yevick closure. A non-linear equation for the effective potential parameter c_0 follows[70] from the excluded volume condition and Eq. (26). For the fractal models specified by ω_q from Eq. (12) it connects the repulsive pseudopotential parameter, c_0, to the packing fraction, $\phi=\varrho_m\sigma^3(2\pi^{d/2}/d2^d\Gamma(d/2))$ (often denoted by η elsewhere), and degree of polymerization, N

$$\phi=(-\varrho_m c_0)^{(d\nu-1)} I^{\nu}(-N\varrho_m c_0), \tag{27a}$$

follows from Eq. (26), where

$$I^{\nu}(y)=a\int_0^{\infty} dx \frac{x^{d-1}}{(y^{-2\nu}+x^2)^{1/2\nu}(1+x^{1/\nu})}. \tag{27b}$$

The physically relevant limit $|\varrho_m c_0 N|\gg 1$ is considered in Eq. (27) and the numerical constant $a=4^{1-d}/(d\Gamma^2(d/2)c_1^{d/2})$. Equation (27) is limited to fractal dimensions $d_F=1/\nu>d/2$ since the presumed independence of the thread direct correlation function, c_q, on q misses the high wave vector cut off provided by the actual c_q from Eq. (26), where $c_q\to 0$ for $q\to\infty$. Consistent with the coarse graining of the thread calculation, only the large N limit of the results will be of interest as microscopic length scales except for the Kuhn segment size σ have dropped out of the description. Equation (27) captures the long wavelength aspects of the competition of local packing and macromolecular connectivity.[70] A polymer melt or dense solution is characterized by a finite, of order unity, value of the (normalized compressibility) S_0 in the limit of large N, where from Eq. (26) $S_0=N/(1-N\varrho_m c_0)\approx -1/\varrho_m c_0$. From Eq. (26) it immediately follows that the pair correlation function, $g(r)=1+h(r)$, has to exhibit a long range (order R_g) correlation hole[2,68,69] on intermediate length scales, $\sigma\ll r\ll R_g$, of the form $-h(r)\propto(\sigma/r)^{d-1/\nu}$.

As only S_0, c_0 and g_d are required for the present study of the entanglement problem, the full liquid structure described by the thread model, Eqs. (26) and (27), will not be specified. In the case of one-component chain solutions and melts, copolymer melts, and binary blends, prior PRISM studies have shown that the thread model description reproduces qualitatively well most of the equilibrium behavior obtained using more chemically realistic models.[68,72] However, the contact value g_d cannot be found from the thread model as the diameter of closest contact has been shrunk to zero for analytic convenience. Nevertheless, a qualitatively reliable[33] estimate can be obtained from the thread pair correlation function evaluated at the Kuhn segment length σ, i.e., $g_d\approx g(\sigma)$. Again in the limit of large N this leads to:

$$g_d=\frac{(-\varrho_m c_0)}{\phi} J^{\nu}(-\varrho_m c_0), \quad \text{where} \tag{27c}$$

$$J^{\nu}(y)=\overline{a}\int_0^{\infty} dx\left(1-\frac{\sin(x)}{x}\right)\frac{x^{d-1/\nu-1}}{(y/c_1^{1/2\nu}+x^{1/\nu})}, \tag{27d}$$

and $\overline{a}=ac_1^{d/2-1/\nu}$. The contact value, which is a measure of intermolecular collisions, saturates at a N independent value for polymer fluids well above the semidilute crossover concentration. Significantly smaller melt values (typically $g_d\approx 0.2$-0.7) compared to dense simple liquids (typically $g_d\approx 2$-5) are obtained as monomers from different molecules are partially screened by the monomers of the probe polymer due to both the macromolecular connectivity and thermal conformational disorder.[68,69]

Microscopic PRISM calculations for chemically realistically modeled chain polymers have shown that the equilibrium structure of polymeric liquids exhibits a number of surprisingly general features.[2,3,68,72] Just these more universal features of the liquid structure are captured in the thread model. Whereas the universal aspect of the correlation hole effect is expected the applicability of the thread model on more local length scales and the observation of rather detail-insensitive mesoscopic correlations are not yet fully understood. However, this success of the thread model for linear chains, and its analytic simplicity, motivate our generalization to different, fractal macromolecular architectures.

Due to the coarse grained nature of the thread model an *a priori* identification of the packing fractions, ϕ, or S_0 with the actual values of real experimental systems is impossible. As the segment excluded volume size is shrunk to zero, the connection of the packing fraction to the actual density is complicated. In order to find the physically relevant thread parameter ranges we use the following procedure. We fix a value S_0^{fix} to define the melt case for different fractal dimensions.[32,33,76] Fixing the static structure factor at zero wave vector may be viewed as a calibration or mapping procedure based on a measurable thermodynamic property, i.e., the dimensionless mean density fluctuations or isothermal compressibility. Under fixed pressure, temperature, and concentration conditions one physically expects S_0 is virtually independent of both N and fractal dimension.[2,3,68,72] The thread model is used to calculate the local packing properties. First, the necessary packing fraction (or osmotic pressure) in order to achieve the intermolecular interpenetration required by this fixed compressibility is found from Eq. (27a). Then, the corresponding contact value g_d is found from Eq. (27c). For the purpose of model calculations we fix a value $S_0^{\text{fix}}=50$ to define the melt.[32,33,76] For chain polymers in a theta solvent, this calibration value has been used previously.[33] Equation (27a) then predicts a simple scaling relation, $S_0\propto\phi^{-2}$, and quantitatively realistic values for the excluded volume interactions as has been discussed previously.[33] It correctly reproduces[33] both the crossover N_e found in melt simulations,[73] and the mean squared intermolecular force felt by a probe polymer in a melt as computed using atomistic PRISM theory. In addition, the calibration procedure results in the experimentally correct prediction of power law polymer density scaling of static and dynamical quantities such as the plateau shear modulus all the way up to the melt.[33,34] This parameter choice issue or ''mapping'' procedure will not affect our main goal of establishing the qualitative variations of the entanglement dynamics with fractal dimension since no adjustable equilibrium structural parameters are involved when macromolecular fractal dimension is varied. We have checked that of order 50% variations in the fixing value, S_0^{fix}, do not affect the results qualitatively.

After calibrating all melts to have a fixed $q=0$ collective structure factor, $S_0\approx 1/(-\varrho_m c_0)$, Eqs. (27) determine the packing fraction ϕ and the contact value g_d as a function of fractal dimension. In the stated limits, $|N\varrho_m c_0|\gg 1$ and $|\varrho_m c_0|\ll 1$, they lead to

$$\phi/(a(-\varrho_m c_0)^{(d\nu-1)}) \to \begin{cases} \dfrac{\pi\nu}{\sin(\pi\nu(d-1/\nu))}, & \text{for } 1 \neq d\nu < 2\,, \\ \left(\dfrac{\ln(-N\varrho_m c_0)}{d} + \ln(d-1) - (d-2) \right), & \text{for } \nu = 1/d. \end{cases} \tag{28a}$$

Although the PRISM equations and the thread limit only deal with statistical averages of two point correlation functions, they indicate that the packing or interpenetration varies strongly with fractal dimension in accord with physical intuition. In order to achieve similar melt compressibilities the packing fractions have to be increased by roughly an order of magnitude when going from open structures, e.g., $d_F = 2$ in $d = 3$, to objects whose fractal dimension coincides with the spatial dimension they are embedded in, $d_F = 1/\nu = d$. Figure 1 shows the numerical solutions of Eq. (27a) for spatial dimension $d = 3$, $N = 10^6$, and for $S_0^{\text{fix}} = 50$. The asymptotic formulae, Eq. (28a), indicate that the case $d_F = d$ differs qualitatively. For smaller fractal dimensions, $d\nu < 1$, melt like compressibilities can be achieved by increasing modestly the packing fraction at fixed N. For fractals where d_F and d are close or equal the segment density has to be dramatically increased in order to force the polymers to interpenetrate and suppress the intra-molecular correlations. In Fig. 1 the results of more microscopic PRISM calculations for some fractal dimensions are included. These numerical calculations solve Eq. (26) with finite hard core diameter, $D = \sigma$, a Percus-Yevick excluded volume closure, $c(r > D) = 0$, and the intramolecular structure determined from the finite summation, Eqs. (3) and (12c). Choosing a uniform lower melt calibration value, $S_0^{\text{fix}} = 35$, is enough to (almost) collapse the thread and numerical calculations, which thereby justifies our use of the thread model within the framework of a Gaussian fractal model.

The trend of less effective intermolecular packing can also clearly be seen from the contact values g_d. Figure 2 demonstrates an order of magnitude decrease in the contact value at fixed structure factor S_0^{fix} in $d = 3$-dimensions as the fractal dimension is increased. Note that the coupling parameter (prefactor) of the RR model effective friction contains g_d^2 Therefore, on general grounds (independent of the use of the thread PRISM) the theory predicts the crossover to entangled dynamics to be shifted to higher molecular weights because of the unavoidable physical fact that macromolecules of larger fractal dimension interpenetrate less. The asymptotic results for $|N\varrho_m c_0| \gg 1$ and $|\varrho_m c_0| \ll 1$ show again that, except for the case of $d_F = d$, the contact values saturate at melt-like values for large N

$$g_d / \left(\frac{\overline{a}}{\phi}(-\varrho_m c_0) \right) \to \begin{cases} \dfrac{\pi/2}{\Gamma(2+2/\nu-d)\sin\left(\dfrac{\pi}{2}(2/\nu-d)\right)}, & \text{for } \dfrac{2}{2+d} < \nu < 2/d, \\ \left(\dfrac{-\ln(-\varrho_m c_0 / c_1^{1/2\nu})}{3(d+2)} + 0.209\ldots \right), & \text{for } \nu = \dfrac{2}{d+2}, \\ (-\varrho_m c_0 / c_1^{1/2\nu})^{-(2-\nu(d+2))} \dfrac{\pi\nu/6}{\sin(\pi\nu(d+2-1/\nu))}, & \text{for } 1/d \leq \nu < \dfrac{2}{d+2}. \end{cases} \tag{28b}$$

At $d_F = d$ the packing fraction which corresponds to our definition of the melt depends logarithmically on N for large N. Of course, for d_F approaching the spatial dimension large finite N corrections to the asymptotic behavior are expected. The numerical results of the full PRISM calculation, rescaled by a constant factor, are included in Fig. 2 and agree nicely with the thread results.

V. DYNAMICS OF ENTANGLED FRACTAL MACROMOLECULES

The dynamical equations of Section III are solved and discussed for different fractal dimensions focussing on spatial dimension $d = 3$. In order to facilitate the presentation examples for some specific fractal dimensions are stated repeatedly. The ideal Gaussian random walk chain case serves as the known cornerstone. Other dimensions are chosen in order to indicate the breadth of variation with $d_F = 1/\nu$. Generally, but not exclusively, monotonic trends with d_F are observed. Due to the existence of a lower limit, d_F^c, below which entanglement effects are inoperative in the theory ($d_F^c = d/2$), we will focus on the range $2 \leq d_F = 1/\nu \leq 3$, which is the most experimentally relevant. This also allows one to use the thread-PRISM model for all fractal dimensions, as it is well defined for $d_F > d/2$.

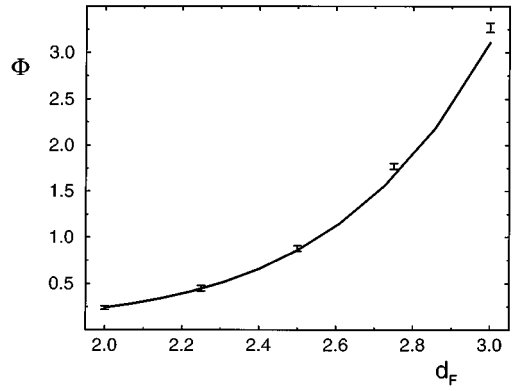

FIG. 1. Packing fractions ϕ in the thread model of Eq. (27a) in $d=3$ dimensions using $N=10^6$ and $S_0^{\mathrm{fix}}=50$. Numerical PRISM results using the Percus-Yevick closure, $c(r>D)=0$, for the same parameters and hard sphere diameter $D=\sigma$ are included with error bars corresponding to $S_0^{\mathrm{fix}}=35\pm5$.

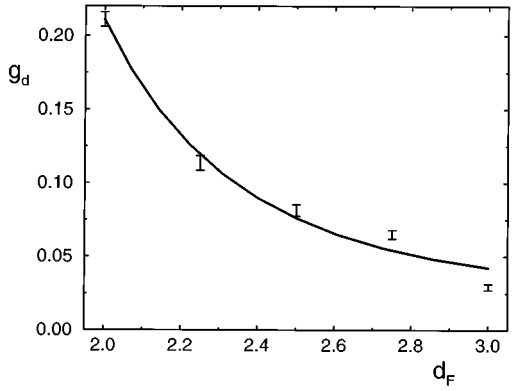

FIG. 2. Contact values g_d in the thread model of Eq. (27c) in $d=3$ dimensions using $N=10^6$ and $S_0^{\mathrm{fix}}=50$. Numerical PRISM results using the Percus-Yevick closure, $c(r>D)=0$, for the same parameters and hard sphere diameter $D=\sigma$ are multiplied by a factor 3.70 and included with errorbars corresponding to $S_0^{\mathrm{fix}}=35\pm5$.

A. Renormalized Rouse model predictions

The mode spectrum of the simplified RR model with a uniform friction function is identical to the one of the Rouse problem.[27] However, a frequency dependent friction coefficient, $\zeta^{(\mathrm{RR})}(z)=1-i\Lambda(z)$, enters, see Eq. (2a). Its dynamics is governed by the Rouse dynamics, which is characterized by the Rouse relaxation time,[44,45] $\tau^{\mathrm{R}}=N^{1+2\nu}$, and has the following limiting behaviors:

$$\Lambda(z)\rightarrow\begin{cases} c_3(-\psi/z)(-iz)^{\frac{\nu(2+d)-1}{1+2\nu}}, \quad \text{for } z\tau^{\mathrm{R}}\gg 1, \quad c_3=\displaystyle\int_0^\infty dx\,\frac{x^{d+1-1/\nu}}{c_1^{(1/2\nu)}+x^{2+1/\nu}c_1^{1/\nu}/d}, \\ i\zeta^{(\mathrm{RR})}=i\psi N^{2-d\nu}c_4, \quad \text{for } z\tau^{\mathrm{R}}\ll 1, \quad c_4=d\displaystyle\int_0^\infty dx\; x^{d-1}\hat{\omega}^2(x). \end{cases} \tag{29}$$

On intermediate time scales there is a power law decrease of the friction function, $\Lambda(t)\propto t^{-x}$, where $x=(\nu(2+d)-1)/(1+2\nu)$ and $x=3/4$ for Gaussian chains in $d=3$-dimensions. The origin of such temporal behavior is fluctuating force contributions from intermediate length scales, $1\gg q\gg 1/R_g$, where the macromolecule exhibits a self-similar structure. The anomalous diffusion which $\Lambda(z)$ leads to is directly connected to the self-similarity of the underlying equilibrium structure. Equation (29) also predicts[30] that the effects of entanglements on the dynamics are not negligible if $\nu<2/d$ or $d_F>d/2$.

The RR model calculates the entanglement effects perturbatively and therefore is expected to apply to weakly entangled systems, or for strongly entangled systems at relatively short times.[28] An appropriate measure for the entanglement transition can therefore be obtained from equating the RR correction to the unperturbed Rouse friction.[33] Two such comparisons are possible from Eq. (29) and define either an entanglement crossover degree of polymerization, N_c' or a crossover time, τ_c. The former criterion implemented in the Markov ($z\rightarrow 0$) limit yields

$$N_c'=(1/\psi c_4)^{1/(2-d\nu)}. \tag{30a}$$

At N_c', the molecule is of a size where the total friction exerted on its center-of-mass due to intermolecular excluded volume forces, or entanglements, has increased to the same level as the friction from fast microscopic degrees of freedom, which are described by the monomer friction coefficient, ζ_0.

The crossover time scale, τ_c, which follows from equating the self-similar spectrum in Eq. (29) to the monomer friction coefficient, $|\Lambda(z=1/\tau_c)|=1$, measures when the short time, Rouse model breaks down due to the temporal build up of entanglement friction effects. In the spirit of an instability analysis, i.e., assuming that at this breakdown of the Rouse description one can still use it to estimate the mean squared displacement, Eq. (18), and the shear modulus, Eq. (21), a corresponding length scale, $r_c\propto\tau_c^{\nu/1+2\nu}$ and crossover degree of polymerization, N_c, can be estimated

$$\tau_c=(\psi c_3)^{-\frac{1+2\nu}{2-d\nu}}\rightarrow N_c=(\psi c_3)^{\frac{-1}{2-d\nu}}/c_5, \tag{30b}$$

where

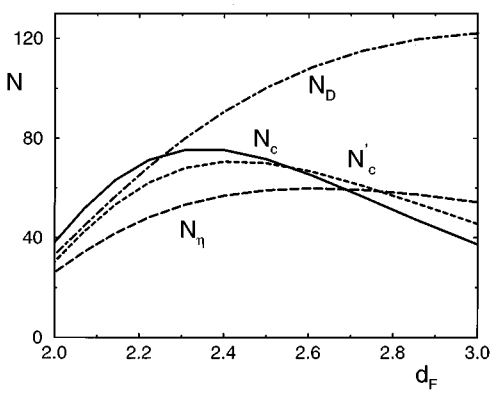

FIG. 3. Crossover degrees of polymerization. From the renormalized Rouse model as defined in Eq. (30b) N_c solid line, or Eq. (30b) N_c' short dashed line. From the polymer mode coupling model as defined for the diffusion coefficient in Eq. (51) N_D chain curve, and for the viscosity in Eq. (53e) N_η long dashed line.

$$c_5=(c_2/2)^{\frac{1}{1+2\nu}}\Gamma(1+1/(1+2\nu))/\pi,$$

and the standard connection from rubber elasticity,[3] $G_c=G^{\mathrm{R}}(\tau_c)=\varrho_m k_B T/N_c$ was used.

The RR model provides the two crossover measures indicating the change of the polymer dynamics due to entanglements. N_c and N_c' are non-equilibrium quantities which by virtue of Eq. (30) are directly connected to the equilibrium input characterizing the probe, Eq. (14), and the liquid structure, Eq. (27). Using the static information from the thread-PRISM calculation one can study N_c and N_c' for different fractal architectures. As discussed in Section III, there still exists an undetermined numerical prefactor in ψ, denoted by A, arising from the coarse graining in the thread limit. We choose $A=0.0182$ in order to recover previous results obtained for $d_F=2$ Gaussian chains in string-PRISM calculations and melt values of $N_c\approx$ 30-40 found in computer simulations of Gaussian chain melts.[33,73] Figure 3 then shows the dependence of N_c and N_c' on fractal dimension. Non-monotonic variation of the latter quantities arises from the monotonic variation of the static parameters for different ν. Gratifyingly, both crossover degrees of polymerization are rather close and vary by less than a factor of 3 as a function of d_F. N_c and N_c' show identical scaling with physical parameters, such as density. Different ways to calibrate the static melt input modify the details of the curves in Fig. 3, but do not destroy the trend of rather close values and the non-monotonic dependence on d_F.

The length scale r_c is a measure of the entanglement distance, signaling when the interchain excluded volume interactions plus connectivity constraints dominate over the bare Rouse dynamics. The values for r_c, $r_c\approx 3\sigma$, which are obtained from the static input are rather small and indicate the restricted validity of the Rouse description in the entangled melt.

The static PRISM input also allows the study of solutions, e.g., the prediction of the dependence of the entanglement parameters on density and solvent quality can be determined.[33] Reducing the density in the PRISM calculations corresponds to concentrated and semi-dilute solutions where an effective Gaussian assumption for the intra-molecular structure is still employed with a density dependent segment length, $\sigma(\varrho_m)$, the details of which depend on solvent quality, fractal architecture, and chemical structure. From the asymptotic results, Eq. (27), of the thread-PRISM calculations simple proportionalities of the entanglement length, r_c, the crossover degree of polymerization, N_c, and the shear or plateau elastic modulus, $G_c=\varrho_m k_B T/N_c$, can be deduced (recall $\phi\propto\varrho_m\sigma^3$)

$$N_c\propto(\sigma/D)^s\begin{cases}\phi^{-r} & \text{for } 2/d>\nu>1/d,\\ (Ne^{-d\phi/a})^{(4-d)/d}\phi & \text{for } \nu=1/d,\end{cases} \tag{31a}$$

$$r_c\propto\sigma(\sigma/D)^{s\nu}\begin{cases}\phi^{-r\nu} & \text{for } 2/d>\nu>1/d,\\ (Ne^{-d\phi/a})^{(4-d)/d^2}\phi^{1/d} & \text{for } \nu=1/d,\end{cases} \tag{31b}$$

where for theta solutions σ is independent of ϕ and $s=2\,dr$ with

$$r=\begin{cases}\dfrac{1}{d\nu-1} & \text{for } 2/d>\nu>2/(2+d),\\ \dfrac{d\nu-2+4\nu}{(d\nu-1)(2-d\nu)} & \text{for } 2/(d+2)>\nu>1/d,\end{cases} \tag{31c}$$

where the dependence on an effective aspect ratio, (σ/D), is denoted as well.

Compared to the relatively weak dependences for Gaussian chains in $d=3$ previously found[33] when $D=\sigma$, $r_c\propto(\varrho_m\sigma^2)^{-1}$, $N_c\propto(\varrho_m\sigma^3)^{-2}$ and $G_c\propto(\varrho_m\sigma^2)^3$, more compact macromolecules show an increased density dependence. For example, at $d_F=(2+d)/2=5/2$, $r_c\propto\sigma(\varrho_m\sigma^3)^{-2}$, $N_c\propto(\varrho_m\sigma^3)^{-5}$ and $G_c\propto\varrho_m(\varrho_m\sigma^3)^5$ result. From the thread considerations it can be expected that rather large corrections to the simple scaling laws, Eq. (31), can be observed for fractal dimensions close to $\nu=2/(2+d)$ and $\nu\to 1/d$. It is also worth noting that the very coarse grained description of the fractal models employed in this work still captures some chemical structure features like the dependence on the local aspect ratio $\Gamma=\sigma/D$. It enters very strongly and is expected to lead to material dependent differences in the plateau shear modulus and the entanglement length in addition to the system-specificity inherent to quantities such as the segmental packing fraction $\phi\propto\varrho_m\sigma^3$. The surprising dependence of the entanglement quantities, Eq. (30), on degree of polymerization if fractal and spatial dimension are equal arises from a property of the PRISM equations mentioned in Section IV: logarithmically increasing with N densities are required in order to force interpenetration and equal bulk compressibility, $S_0\propto N\exp(-\phi d/a)$, in this case. Note, however, that the exponential density dependence clearly dominates for concentrated solutions and melts, as $a(d=3)\approx 1.10$.

This extension of melt results to solutions clearly bears an important caveat, even for theta solutions, where Gaussian intra-molecular statistics is appropriate. The model of a solution obtained in this way does not include hydrody-

namic interactions. The results therefore can be applied only if the hydrodynamic screening length is sufficiently small.

The assumption of Gaussian intra-molecular structure might seem to rule out predictions for good solutions, where the long range excluded volume interactions drastically change the intra-molecular structure. However, using the blob picture developed by de Gennes[2] and the Cates and Muthukumar extension of the Flory approach to the excluded volume effects of fractal molecules,[44,45] further progress is possible. As done for Gaussian chains, the de Gennes blob picture can be incorporated into the thread-PRISM calculation by identifying the effective segment length scale with the blob size,[33] ξ_b. The central idea is to consider the solution of self avoiding fractals as a melt of Gaussian fractals of larger units, the so-called blobs.[2] Within the blob, the molecule is swollen due to the excluded volume interaction, the melt of blob-molecules, however, is ideal, following Flory's argument. Therefore, the thread-PRISM equations, which are input with Gaussian structure, are considered to describe macromolecules made up of blobs and the length scales entering them, i.e., σ, are identified with the blob size, ξ_b. The intermolecular excluded volume condition, $g(r<D)=0$, in this case presumes that the molecule is in the dilute, self avoiding limit within the blob. Within the blob, one can use the calculations of Refs. 44 and 45 for the mass scaling exponent, $\overline{\nu}$, of fractals with intramolecular excluded volume interactions. From minimizing the single macromolecule free energy, $F/k_BT \propto (R^2/R_0^2)+v(N^2/R^d)$, composed of the Gaussian elastic energy, where $R_0 \propto N^{\nu}$, and the pairwise repulsive interaction of strength v, one obtains the dilute solution exponent,[44,45] $\overline{\nu}=2(1+\nu)/(2+d)$. The scaling of the blob size, ξ_b, with density can be obtained from the standard scaling argument for the radius of gyration at the dilute to semi-dilute crossover: $R_g \propto N^{\nu} f_R(\varrho_m/\varrho_m^*)$, requiring $f_R(0)=1$ and the scaling $R_g \propto \xi_b N^{\nu}$ above the semi-dilute crossover,[2] $\varrho_m^* \ll \varrho_m \ll 1$. Here, the polymer overlap concentration, ϱ_m^* is $\varrho_m^* \propto N/R_g^d \propto N^{1-\overline{\nu}d}$, which leads to the result for the dependence of ξ_b on density

$$\xi_b \propto \varrho_m^{-\frac{2-\nu d}{d+2\nu d-2}}. \tag{32}$$

In contrast to the weak density dependence, $\xi_b \propto \varrho_m^{-1/8}$, for Gaussian chains in $d=3$-dimensions,[2] stronger dependences are found for more dense fractal molecules, e.g., $\xi_b \propto \varrho_m^{-1/3}$ if $d_F=d=3$. The results for the density dependence of the crossover quantities characterizing the entanglement effects in good solvents can now be obtained from Eq. (30) by replacing the monomer length scales, D and σ, with the blob size, Eq. (32)

$$G_c \propto \frac{\varrho_m}{N_c}, \quad N_c \propto \begin{cases} \varrho_m^{-\frac{d+2}{d+2\nu d-2}} & \text{for } \frac{2}{d} > \nu > \frac{2}{2+d} \\ \varrho_m^{-\frac{(d+2)(d\nu-2+4\nu)}{(d+2\nu d-2)(2-d\nu)}} & \text{for } \frac{2}{2+d} > \nu > \frac{1}{d}, \end{cases} \tag{33a}$$

where

$$r_c \propto \begin{cases} \varrho_m^{-\frac{2+2\nu}{d+2\nu d-2}} & \text{for } \frac{2}{d} > \nu > \frac{2}{2+d} \\ \varrho_m^{-\frac{(2-\nu d)^2+\nu(d+2)(d\nu-2+4\nu)}{(d+2\nu d-2)(2-d\nu)}} & \text{for } \frac{2}{2+d} > \nu > \frac{1}{d}. \end{cases} \tag{33b}$$

Comparing the predicted density dependences for theta solutions, Eq. (30), and good solvents, Eq. (33), only relatively small differences are observed for Gaussian chains. For $\nu=1/2$ in good, $d=3$-dimensional solutions, $r_c \propto \varrho_m^{-3/4}$, $N_c \propto \varrho_m^{-5/4}$, and $G_c \propto \varrho_m^{9/4}$, are found.[33] For denser objects, however, good and theta solvents cases differ more because of the larger swelling in the intra-molecular equilibrium structure. The effective packing fraction, $\phi \propto \varrho_m \xi_b^d$, in theta-solvents, depends more weakly on monomer density for more compact objects,

$$\phi \propto \varrho_m^{(d\nu-1)\frac{d+2}{d+2\nu d-2}}.$$

For example the following dependences hold, $r_c \propto \varrho_m^{-14/17}$, $N_c \propto \varrho_m^{-25/17}$, and $G_c \propto \varrho_m^{42/17}$ for a fractal dimension $d_F=1/\nu=5/2$ in a 3-dimensional good solvent, and even for $d_F=1/\nu=d=3$, the exponential density dependence is removed resulting in $r_c \propto \varrho_m^{-14/27}$, $N_c \propto \varrho_m^{-5/9}$, and $G_c \propto \varrho_m^{14/9}$ for a good solvent. Again, it has to kept in mind, that hydrodynamic interactions are neglected in these results.

It is easily possible to obtain all the dynamical quantities listed in Section II within the RR model. As is well known from prior work on linear chains, one finds strong corrections to the Rouse dynamics but not a qualitatively correct description of strongly entangled systems.[27] Only the PMC model leads to a strong enough slowing down of translational diffusion and the internal conformational modes to correctly predict the N-dependence of the center-of-mass diffusion constant and a two step process in the intra-molecular stress relaxation. The only dynamical input to the PMC theory is the friction function $\Lambda(z)$ of the RR model. Thus the results of this subsection allow the derivation of the entangled dynamics predictions of the PMC model.

Previous analysis of the RR or PMC model has used slightly different technical approximations for the dynamics entering the respective memory functions. Our analysis is in agreement with the usage of Ref. 30 except for negligible differences in the numerical prefactors and of the final decay in $\Sigma(t)$, which will be commented on below.

B. Time scales and transport coefficients of the polymer mode coupling theory

The dynamics of entangled macromolecules in the large N limit is described by the PMC model, which is defined by the memory functions $\Sigma(z)$, Eq. (17b), affecting the center-of-mass motion, and $m^{\lambda}(z)$, Eq. (19), describing the dynamics of the internal modes. The latter can be separated into a

uniform contribution, $\Sigma'(z)$, and a mode-dependent part, $M(z)$, if the approximate expression Eq. (24d) for the intramolecular structural density of states is used; i.e., $m^{\lambda}(z)=\Sigma'(z)+\lambda^{1+2\nu}M(z)$ where

$$\Sigma'(z)=\psi' c_1^{1/2\nu}\int_0^{\infty} dk\ k^{d+1+1/\nu}\omega_k^2 \frac{-1}{z+\dfrac{i(k^2/d\omega_k)}{1-i\Lambda(z)}}, \quad (34a)$$

$$M(z)=\psi'(d/c_2)\int_0^{\infty} dk k^{d-1}\omega_k^2 \frac{-1}{z+\dfrac{i(k^2/d\omega_k)}{1-i\Lambda(z)}}, \quad (34b)$$

The difference between $\Sigma(z)$ and $\Sigma'(z)$, which has been neglected in previous studies, arises due to different approximations in diagonalizing Eqs. (1). As will be shown below, however, this has nontrivial consequences only for the final long time tail of $\Sigma(z)$ which is of essentially no practical significance.

For entanglements, the shortest time scale of interest is the crossover time, τ_c, determined in Eq. (30b). For longer times, or smaller frequencies, $|\Lambda(z)|\gg 1$ follows in Eq. (34), i.e., the bare friction is negligible. In the Rouse problem, there enters the familiar Rouse time,[44,45] which scales with degree of polymerization as $\tau^{\mathrm{R}}=N^{1+2\nu}$. Another, longer time scale, τ^{RR}, arises in the RR model. It is the characteristic relaxation time for the contributions to the PMC force fluctuations arising on the length scale of the macromolecule[27,30]

$$\tau^{\mathrm{RR}}=c_4\psi N^{3-(d-2)\nu}. \quad (35)$$

The τ^{RR} time scale shows up in the long time dynamics only as a crossover time, where the longest lasting, small ($\propto 1/R_g$) wave vector contributions to the PMC-friction functions start decaying. Due to the small weight of these long wavelength modes in the uniform memory functions, $\Sigma(z)$ and $\Sigma'(z)$, no new, longer time scale results from them. As will be seen later, however, the M-memory function leads to a new, longest time scale, τ_D, which dominates the internal mode relaxation and can be defined from the Markovian limit[28,30] of $M(z=0)$

$$\tau_D=\psi\psi' N^{5-2\nu(d-1)}c_6, \quad (36)$$

where

$$c_6=(d^2c_4/2)\int_0^{\infty} dx\ x^{d-3}\hat{\omega}^3(x).$$

For Gaussian chains in $d=3$ dimensions, we recover the known results,[27,28] $\tau^{\mathrm{RR}}\propto N^{5/2}$ and $\tau_D\propto N^3$. For larger fractal dimensions higher values for the exponents are found. For example, in the limit of $d_F=1/\nu\to d=3$, $\tau^{\mathrm{RR}}\propto N^{8/3}$ and $\tau_D\propto N^{11/3}$, are obtained.

Using the thread-PRISM calculations, one can determine the polymer density and statistical segment length scaling of the final disentanglement or terminal relaxation time, τ_D. For theta solvents, where σ is constant, and for good solvents, where $\sigma\approx\xi_b(\varrho_m)$ from Eq. (32), one finds

$$\tau_D\propto N^{5-2\nu(d-1)}g_d^2\propto N^{5-2\nu(d-1)}\begin{cases}(\varrho_m\sigma^d)^{\frac{4-2d\nu}{d\nu-1}}, & \text{for } \dfrac{2}{d}>\nu>\dfrac{2}{2+d},\\ (\varrho_m\sigma^d)^{\frac{4-2d\nu}{d\nu-1}}, & \text{for } \dfrac{2}{2+d}>\nu>\dfrac{1}{d},\end{cases} \quad \text{for theta solv.,} \quad (37a)$$

$$\tau_D\propto N^{5-2\nu(d-1)}g_d^2\propto N^{5-2\nu(d-1)}\begin{cases}\varrho_m^{\frac{(4-2d\nu)(d+2)}{d+2d\nu-2}}, & \text{for } \dfrac{2}{d}>\nu>\dfrac{2}{2+d},\\ \varrho_m^{\frac{4\nu(d+2)}{d+2d\nu-2}}, & \text{for } \dfrac{2}{2+d}>\nu>\dfrac{1}{d},\end{cases} \quad \text{for good solv.} \quad (37b)$$

For Gaussian chains in $d=3$, this predicts: $\tau_D\propto N^3\varrho_m^2$, in theta solvents, and $\tau_D\propto N^3\varrho_m^{5/4}$, in a good solvent.[34] For denser fractal objects higher powers in degree of polymerization and density are obtained; e.g., $\tau_D\propto N^{11/3}g_d^2$ for $d_F=d=3$ follows, where g_d depends exponentially on the density, $g_d^2\propto e^{4\varrho/a}$ for theta solvents, and $g_d^2\propto\varrho_m^{20/9}$ for good solvents.

The four time scales, τ_c, τ^{R}, τ^{RR} and τ_D, separate windows of different dynamical behavior, which will be characterized below by the leading (power-law) time or frequency dependent term. Of course, clear observation of the leading terms requires a wide separation of the time scales limiting the appropriate window. Although this is achieved in the $N\to\infty$ limit, for realistic N values large finite size corrections are expected.[31,32]

Another quantity of interest is the center-of-mass translational diffusion coefficient, D, which can be obtained from the Σ-memory function in the Markovian limit[28,30]

$$1/D=\psi\psi' N^{5-2d\nu}c_4^2. \quad (38)$$

The scaling, $D \propto N^{-2}$, for Gaussian chains in $d=3$ dimensions is recovered, and again larger exponents are observed for smaller ν; e.g., $D \propto N^{-13/5}$ for $d_F=5/2$ and $D \propto N^{-3}$ for $d_F=1/\nu=d$. The density and statistical segment length scaling of the diffusion coefficient can simply be obtained from τ_D, Eq. (37), by noting that the product of diffusion coefficient and internal time scale divided by R_g^2 depends on fractal and spatial dimension only, but not on other structural parameters

$$\frac{D\tau_D}{R_g^2}=f^{(\mathrm{SE})}(\nu,d)=\frac{d}{2}\frac{\int dx x^{d-3}\hat{\omega}^3(x)}{\int dx x^{d-1}\hat{\omega}^2(x)}. \tag{39}$$

This ''Stokes-Einstein'' like ratio shows that in the PMC model the slow dynamics of different processes is connected by an underlying common diffusion process determining the friction. This feature is in agreement with the reptation/tube model; indeed, the ratio $D\tau_D/R_g^2$ is predicted to be 1/4 by the tube model which is remarkably close to the PMC prediction of $\approx$0.2 (see Fig. 4). As two different memory functions, Σ and M, determine τ_D and D, respectively, this result is non-trivial and can be traced back to the use of the coherent single macromolecular dynamic structure factor of the RR model in the PMC friction functions. The above ratio is shown in Fig. 4 and varies monotonically with fractal dimension but only by a factor less than 3. Let us recall that time scales in this section are given in units of $\tau_0=\sigma^2/dD_0$; using the dimension-carrying, experimental variables τ_D, D and R_g, Eq. (39) changes to $D\tau_D/R_g^2=f^{(\mathrm{SE})}/d$. It is this ratio which is shown in Fig. 3.

Before proceeding to discuss finite frequency properties, it is instructive to compare the above asymptotic large N predictions of PMC theory with the analogs of the reptation/tube approach. If the Gaussian fractals can be thought of as linear, flexible polymers, the most naive generalization of the tube model ansatz makes the prediction

$$\tau_D^{\mathrm{rep}} \propto L^2/D^{\mathrm{R}} \propto N^2/D^{\mathrm{R}} \propto N^3, \tag{40a}$$

since the terminal relaxation is driven by the destruction of the tube of contour length $L \propto N$ via the coherent reptative motion of the probe polymer described by the center-of-mass diffusion coefficient of the Rouse model, $D^{\mathrm{R}} \propto 1/N$. This result holds for *all* values of fractal, d_F, and spatial, d, dimension. It agrees with PMC theory only if $d_F=1/\nu=(d-1)$, i.e., in $d=3$ dimensions *only* for ideal random walk coils. Similarly, the tube model prediction for the translational diffusion coefficient follows from the underlying diffusive process

$$D^{\mathrm{rep}} \propto R_g^2/\tau_D \propto N^{-3+2\nu}, \tag{40b}$$

In $d=3$, this result agrees with Eq. (38) only for the cases of ideal coils ($\nu=1/2$) and rigid rods ($\nu=1$, where the Rouse result replaces Eq. (40b)). PMC theory also predicts a significant dependence of the entanglement friction on spatial dimension. For example, in a $d=2$ dimensional melt of self-avoiding walk random coils ($\nu\approx 3/4$) PMC predicts $\tau_D \propto N^{7/2}$ and again $D \propto N^{-2}$, the latter in accidental agreement with the familiar $d=3$ dimensional ideal linear chain result even though the relaxation time scaling differs. On the other hand, the tube model yields $\tau_D \propto N^3$ and $D \propto N^{-3/2}$. Recent simulations by Slater and Wu[74] of swollen coils in a $d=2$ model gel appear to support the PMC result for D. PMC theory also predicts that *all* entanglement effects become irrelevant above a critical spatial dimension, d_c, given by $d_c=2/\nu$. For $d>d_c$, the $D \propto N^{-1}$ and $\tau_D \propto \tau^{\mathrm{R}} \propto N^{1+1/2\nu}$ Rouse laws are recovered. Thus for ideal linear chains entanglements are predicted to be inoperative above 4 spatial dimensions. Let us also note that this prediction clearly shows the different physical contents of the PMC theory as compared to the cooperative cluster theory of Douglas and Hubbard,[7] where the Rouse model is recovered in the limit $d\to\infty$.

There is a simple geometric interpetration of both the N-scaling and the prefactor $\psi\psi'$ of the diffusion constant in Eq. (38). It is based on the formally exact relation

$$D^{-1} \propto N[1+(-i\Sigma(z=0))],$$

where,

$$-i\Sigma(z=0)=\frac{\beta}{d\zeta_0 N}\sum_{\alpha\beta}^{N}\int_0^\infty dt\langle \vec{F}_\alpha^{Q}(t)\cdot\vec{F}_\beta(0)\rangle. \tag{41}$$

From Eq. (17b) one can write $\Sigma(z=0) \propto (g_d N^{2-d\nu})^2$. The quantity $N^{2-d\nu}$ is proportional to the number of binary contacts between a pair of interpenetrating fractals in d dimensions. The factor g_d quantifies the intermolecular contact probability or strength of the local excluded volume forces. Thus, the entanglement friction contribution is proportional to the *square* of the product of these factors, a connection which appears natural because the four point force-force correlation function in Eq. (41) describes excluded volume interactions or constraints exerted on two probe segments by the surrounding matrix. Equations (37) then follow immediately from the diffusion-like relation that $\tau_D \propto R_g^2/D$. The latter corresponds to the intuitive idea that global macromolecular and stress relaxation is coupled on a time scale proportional to the time required for the probe to diffuse a distance of order its size. The irrelevance of entanglements

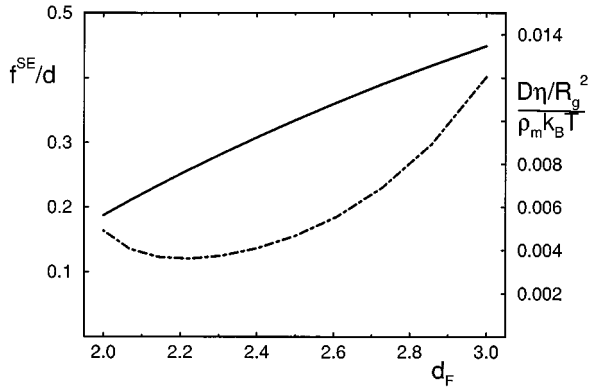

FIG. 4. Transport coefficient ratio, $D\tau_D/R_g^2$ Eq. (39) (using dimension-carrying variables), in $d=3$ dimension and for different fractal dimensions (solid line and left scale). The normalized Stokes-Einstein ratio, $D\eta/(R_g^2\varrho_m k_B T)$, is shown as chain curve and refers to the right scale.

for $d>d_c$ corresponds to the vanishing of the number of two-macromolecule binary contacts in the large N limit.

C. Finite frequency predictions of PMC theory

Using the result, Eq. (29), for the RR-friction function, $\Lambda(z)$, one can easily find the leading asymptotes of the PMC-memory functions in the different time windows. At the shortest times, $t\ll\tau_c$, the dynamics is dominated by the local unentangled Rouse modes, as discussed in the next section. Only results which are (qualitatively) unaffected by them will be listed below. For the center-of-mass memory function one finds the following leading order behaviors:

$$\Sigma(z)\propto\begin{cases}\dfrac{-\psi'}{z}(\psi(-iz)^x)^x & 1/\tau^{\mathrm{R}}\ll z\ll 1/\tau_c,\\ \dfrac{-\psi'}{z}(\psi N^{2-d\nu}(-iz))^x & 1/\tau^{\mathrm{RR}}\ll z\ll 1/\tau^{\mathrm{R}},\\ (i/ND) & z\ll 1/\tau^{\mathrm{RR}},\end{cases}\quad\text{where } x=\frac{\nu(d+2)-1}{1+2\nu}. \tag{42a}$$

The Laplace back-transformation to $\Sigma(t)$ can easily be done for these power laws using: $\mathrm{LT}[t^{-x}](z)=-1/z\,\Gamma(1-x)\times(-iz)^x$. The fractal time exponent, x, in Eq. (42a) again arises from the self-similar equilibrium structure on intermediate length scales. It equals $x=3/4$ for ideal Gaussian chains,[30] and drops to $x=2/5$ for $d_F=1/\nu\to d=3$. The final crossover in $\Sigma(z)$ to the Markovian limit for small frequencies is governed by the long time tail in $\Sigma(t)$. The rather rapid behavior, $\Sigma(t\gg\tau^{\mathrm{RR}})\propto N^{-(d+1)}(t/\tau^{\mathrm{RR}})^{-(d+2)/2}$, leads to almost regular behavior in $\Sigma(z)$ for $z\tau^{\mathrm{RR}}\ll 1$. From Eqs. (2a) and (29)

$$\Sigma(z)\to(i/ND)(1+i\overline{a}(-iz\tau^{\mathrm{RR}})+i\overline{b}N^{-(d+1)}\times(-iz\tau^{\mathrm{RR}})^{d/2}+\ldots),\quad\text{for } z\tau^{\mathrm{RR}}\ll 1. \tag{42b}$$

These results immediately determine the center-of-mass motion via Eq. (17a). Anomalous diffusion is found in a broad, N-dependent intermediate time window, $\tau_c\ll t\ll\tau^{\mathrm{RR}}$, where the center-of-mass mean squared displacement increases from $\Phi(\tau_c)\approx r_c^2$ to $\Phi(\tau^{\mathrm{RR}})\approx N^{-(2-d\nu)}R_g^2$

$$\Phi(t)\propto\begin{cases}2t/N & t\ll\tau_c,\\ t^{\left(\frac{\nu(d+2)-1}{1+2\nu}\right)^2}/N & \tau_c\ll t\ll\tau^{\mathrm{R}},\\ t^{\left(\frac{\nu(d+2)-1}{1+2\nu}\right)}/N^{(2-d\nu)\left(\frac{\nu(d+2)-1}{1+2\nu}\right)} & \tau^{\mathrm{R}}\ll t\ll\tau^{\mathrm{RR}},\\ 2Dt & \tau^{\mathrm{RR}}\ll t.\end{cases} \tag{43}$$

Due to the relatively weak coupling of the internal modes to the center-of-mass, simple diffusive behavior is found already for distances smaller than the size of the molecule (in the asymptotic large N limit). Equation (43) also justifies the use of D as center-of-mass translational diffusion coefficient in Eq. (38). In $d=3$ dimensions the anomalous diffusion varies in the range $t^{9/16}/N$ to $t^{4/25}/N$ in the first time window, $\tau_c\ll t\ll\tau^{\mathrm{R}}$, and $t^{3/4}/N^{3/8}$ to $t^{2/5}/N^{2/5}$ in the second window, $\tau^{\mathrm{R}}\ll t\ll\tau^{\mathrm{RR}}$, for the fractal dimensions $d_F=1/\nu=2$ and $d_F=3$, respectively.

The second memory function arising from uniform drag on all segments, $\Sigma'(z)$ from Eq. (34a), agrees with $\Sigma(z)$ in the intermediate frequency window $z\tau^{\mathrm{RR}}\gg 1$. For smaller frequencies, it differs somewhat,

$$\Sigma'(z)\to(i/ND')(1+i\hat{a}(-iz\tau^{\mathrm{RR}})+i\hat{b}(-iz\tau^{\mathrm{RR}})^2+i\hat{c}N^{-1}(-iz\tau^{\mathrm{RR}})^{\frac{\nu d+1}{2\nu}}\ldots)\quad\text{for } z\tau^{\mathrm{RR}}\ll 1. \tag{44}$$

It exhibits an even weaker long time tail, $\Sigma'(t\gg\tau^{\mathrm{RR}})\propto(\tau^{\mathrm{RR}}/t)^{\frac{\nu(d+2)-1}{2\nu}}/N$. As expected from the discussion of the internal self-similar structure and the resulting spectral densities, the uniform drag described by Σ or Σ' is identical, as long as it is dominated by the internal degrees of freedom. Small differences only are found when the long range, lowest lying contributions in the wave vector integrals dominate, i.e., for $z\tau^{\mathrm{RR}}\ll 1$. Most importantly, however, the scaling of the zero frequency transport coefficient is identical, $D\propto D'$.

The M-memory function describes entanglement effects on the internal mode dynamics relevant to stress and conformational relaxation and differs drastically from the uniform friction functions Σ and Σ'. This mathematically arises from the large weight attributed to the small wave vector range $(qR_g\approx 1)$ in the integration in Eq. (34b) arising from the connectivity constraints which enter via $\omega_{\alpha\beta}^{-1}(q)$ in Eq. (4a). Up to times of the order of τ^{RR}, $M(t)$ is effectively frozen

(for $d\nu<2$) at its initial value, which scales with degree of polymerization, N

$$M(t)\dot{=}M_0=\psi' N^{2-d\nu}\frac{c_4}{c_2} \quad \text{for } t\ll\tau^{\mathrm{RR}}. \tag{45a}$$

Note the factor $N^{2-d\nu}$ which is associated with the number of binary pair-molecule contacts. From Eqs. (29) and (34b) one easily obtains the time dependent corrections, $\mu(z)$, to the constant M_0 (which in Laplace-space shows up as a $-z^{-1}$ contribution)

$$\mu(z)=M(z)-\frac{-M_0}{z}\propto\begin{cases}\dfrac{-\psi' c_7}{z}(c_3\psi(-iz)^{\frac{\nu(d+2)-1}{1+2\nu}})^{-\frac{2-d\nu}{1+2\nu}}, & 1/\tau^{\mathrm{R}}\ll z\ll 1/\tau_c,\\ \dfrac{-\psi' c_7}{z}(c_4\psi N^{2-d\nu}(-iz))^{-\frac{2-d\nu}{1+2\nu}}, & 1/\tau^{\mathrm{RR}}\ll z\ll 1/\tau^{\mathrm{R}},\end{cases} \tag{45b}$$

where the coefficient equals

$$c_7=[d^{\nu}/c_1^{1/2}]^{(d+4)/(2\nu+1)}(2-d\nu)\pi\nu \Big/ \left\{[(d+2)\nu-1](2\nu+1)\times dc_2\sin\left[\frac{\pi(\nu(d+2)-1)}{2\nu+1}\right]\right\}.$$

Only for $t/\tau^{\mathrm{RR}}\approx 1$, does the memory function, $M(t)$, start to decay appreciably. The long time tail, $M(t\gg\tau^{\mathrm{RR}})\propto N^{2-d\nu}(\tau^{\mathrm{RR}}/t)^{d/2}$, translates into an anomalous approach of $M(z)$ to its Markovian value

$$M(z)\to\frac{i2\tau_D}{c_2}+\frac{-\psi' c_8}{z}N^{2-d\nu}(-iz\tau^{\mathrm{RR}})^{d/2}+\ldots \quad \text{for } z\tau^{\mathrm{RR}}\ll 1, \tag{45c}$$

where the coefficient equals

$$c_8=\frac{d}{2c_2}\frac{\pi}{\sin(\pi d/2)} \quad \text{for } d>2.$$

Note, that the powers of the final ($t\gg\tau^{\mathrm{RR}}$) long time tails of the two memory functions (Σ and M) differ but depend on the spatial dimension only. Whereas the long time tail in the center-of-mass friction function is familiar from colloidal systems,[42] the one in the internal mode friction function has no counterpart for rigid, spherical particles.

One can estimate a characteristic frequency for the PMC-memory functions from the above considerations. Defining it by the position of the maximum in the loss part[75] of the memory functions, $M''(\omega)$ or $\Sigma''(\omega)$, respectively, one finds, that the characteristic time scales of the Σ- and Σ'-memory functions are N-independent and of microscopic order, whereas $M(t)$ relaxes with a characteristic time of the order of the RR-model time, τ^{RR}. This slow decay of $M(t)$ leads to the appearance of a low-lying dynamical process and an apparent non-ergodicity for stress and conformational relaxation (plateau), identified with the entanglement process. Note, that this is a prediction, not an assumption, of the theory.

The near arrest of the internal-mode memory function has important consequences. First, it causes a non-relaxing part in the PMC-mode correlator for finite λ and for times short compared to τ^{RR}

$$C^{\lambda}(z)=\frac{M_0c_2}{1+M_0c_2}\frac{-1}{z}+\frac{1}{1+M_0c_2}\frac{-1}{1-\dfrac{\lambda^{1+2\nu}(M_0+1/c_2)}{(-z\Sigma'(z))+\lambda^{1+2\nu}(-z\mu(z))}}, \quad \text{for } z\tau^{\mathrm{RR}}\gg 1$$
$$\dot{=}\frac{-1}{z}+\frac{1}{M_0c_2z}\frac{1}{1-\dfrac{z\mu(z)}{M_0}-\dfrac{z\Sigma'(z)}{\lambda^{1+2\nu}M_0}} \quad \text{for } M_0\gg 1. \tag{46a}$$

Second, because of the N-scaling of the initial value M_0 the slow part in $C^{\lambda}(t)$ is of order unity for internal modes, $\lambda\gg\lambda_c\propto 1/N$. This has been used in the second approximate equality in Eq. (46a), which holds for $M_0\gg 1$ and $M_0\lambda^{1+2\nu}=$ fixed. The small-time dependent correction to the plateau will be denoted by $\Delta^{\lambda}(t)$. Its leading asymptotes in the intermediate frequency window depend on the mode index λ and can easily be obtained from the results for Σ' and μ in Eqs. (42) and (45),respectively. For longertimes, $t\gg\tau^{\mathrm{RR}}$, the Markovian limit in the friction functions applies

and the arrested part of $C^{\lambda}(t)$ decays exponentially

$$C^{\lambda}(t)=e^{-(t/2\tau_D)/(1+u(N\lambda)^{-(1+2\nu)})}\approx e^{-(t/2\tau_D)} \quad \text{for } t\gg\tau^{\mathrm{RR}}, \tag{46b}$$

where the uniform relaxation rate is obtained for intermediate modes, $\lambda\gg\lambda_c\approx\pi/N$; the constant is $u=c_2(2\nu+1)\times(2\nu+2)/f^{\mathrm{SE}}(\nu,d)$. The final dynamics in the PMC correlator over a wide frequency range differ drastically from the Rouse or RR-model results, as the dominance of the internal memory function, $M(z)$, causes the mode-dependence to cancel for internal modes. A rather non-trivial consequence, ultimately of the Fourier transformed structural correlations, ω_q^{λ} in Eq. (19), is the arrest of the internal modes for intermediate times, in conjunction with only smaller slowing down of the center-of-mass motion. This prediction of continued (but anomalous) translational diffusion, but near complete arrest of orientational and stress relaxation, is the hallmark of entangled dynamics and is in qualitative agreement with the reptation/tube ansatz.

$$\phi(t)\propto\begin{cases} t^{2\nu\left(\frac{(\nu(d+2)-1)^2}{(1+2\nu)^3}\right)}/N^{(2-d\nu)/(1+2\nu)} & \tau_c\ll t\ll\tau^{\mathrm{R}},\\ t^{2\nu\left(\frac{\nu(d+2)-1}{(1+2\nu)^2}\right)}/N^{\frac{(4-2d\nu)(1+\nu^2(d+2)-\nu)}{(1+2\nu)^2}} & \tau^{\mathrm{R}}\ll t\ll\tau^{\mathrm{RR}},\\ 2Dtv,\ v>1 & \tau^{\mathrm{RR}}\ll t\ll\tau_D,\\ 2Dt & \tau_D\ll t. \end{cases} \tag{47}$$

The averaged monomer mean squared displacement follows the center-of-mass motion only for times longer than the terminal relaxation time, τ_D. τ_D can also be determined by $\phi(\tau_D)=R_g^2$ The cut-off, $\lambda_c\propto\pi/N$, introduced into the spectral density affects the time window $\tau^{\mathrm{RR}}\ll t\ll\tau_D$ only. This stresses that the diffusion for shorter times is caused by the self-similar macromolecular structure. The anomalous exponents for Gaussian chains in $d=3$-dimensions have been derived previously,[30] $t^{9/32}/N^{1/4}$ and $t^{3/8}/N^{7/16}$, and can be compared to the predictions from the reptation model, $t^{1/4}$ for $\tau_c\ll t\ll\tau^{\mathrm{R}}$ and $t^{1/2}/N^{1/2}$ for $\tau^{\mathrm{R}}\ll t\ll\tau_D$. A more strongly hindered dynamics in the PMC model for short times is evident, although this conclusion unambiguously applies in the hypothetical $N\to\infty$ limit, only. For more compact fractal objects, the short time dynamics is even more sluggish, as the denser structure apparently results in more entanglements due to enhanced contacts; for example, $t^{8/125}/N^{3/5}$ for $\tau_c\ll t\ll\tau^{\mathrm{R}}$, and $t^{2/15}/N^{11/15}$ for $\tau^{\mathrm{R}}\ll t\ll\tau^{\mathrm{RR}}$, is obtained in the limit of $d_F=1/\nu=d=3$.

The averaged mean squared displacement, $\phi(t)$, also determines the incoherent dynamic structure factor in the Gaussian approximation, Eq. (10). The coherent intramolecular structure factor in the PMC model exhibits the required center-of-mass diffusion in the long time and small wave vector regime

$$\omega^{\mathrm{coh}}(q,t)\to Ne^{-\frac{q^2}{d}Dt},\quad \text{for } t\gg\tau_D \quad\text{and}\quad qR_g\ll 1. \tag{48a}$$

The averaged segmental mean squared displacement, Eq. (18), can easily be obtained from the limiting results of the memory functions, Eqs. (42), (44), and (45). Manipulating Eq. (18) to

$$\phi(z)-\Phi(z)=\frac{-2}{z}\frac{Y(z)}{(-iz)(1-i\Sigma'(z))}\times\int_{\lambda_c/Y(z)}^{\infty}\frac{ds}{\pi}\frac{1}{1+s^{1+2\nu}},$$

$$\text{where } Y(z)=\left(\frac{(-iz)(1-i\Sigma'(z))}{1/c_2-M(z)}\right)^{1/(1+2\nu)},$$

the different frequency windows can be identified and the asymptotic expansions used to find the leading terms in $\phi(t)$. Laplace back-transforming to the time domain one obtains

In the self-similar range, $qR_g\gg 1$, Eq. (23) shows that a reasonable approximation for ω^{coh} is

$$\omega^{\mathrm{coh}}(q,t)\to 1/(q^2c_1)^{1/2\nu}e^{-(q^2/2d)\,\phi(t)},\quad \text{for } qR_g\gg 1. \tag{48b}$$

Corrections to the second approximate result can only be studied numerically. As discussed previously,[27,28] the use of a linear equation-of-motion theory, and hence a Gaussian-process description, is more uncertain for nonlinear, q-dependent correlation functions such as $\omega^{\mathrm{inc}}(q,t)$ and $\omega^{\mathrm{coh}}(q,t)$.

The arrested amplitude in the PMC correlator, C^{λ}, also leads to the appearance of a plateau in the shear modulus for intermediate times, $\tau_c\ll t\ll\tau^{\mathrm{RR}}$. As the arrested amplitude in C^{λ} is much larger than the dynamical part, $|\Delta^{\lambda}(t)|\ll C^{\lambda}(t)$ for internal modes in this time window, one can expand any correlation function which is a polynomial in C^{λ}, e.g., the stress modulus, Eq. (21), or the radius of gyration correlator,

Eq. (22). It is an unrealistic result of the PMC model that even very local modes, $\lambda \approx \pi$, are arrested by the entanglements, which only are effective for length scales larger than r_c, as has been seen in the RR analysis. Therefore, the mode independent static amplitudes in $C^{\lambda}(t)$ are cut off at a mode index π/N_e, where for simplicity we identify $N_e = N_c$ from Eq. (30). For intermediate times the entanglement plateau in the shear modulus, $G(t) \approx G_c$, follows. Including the dominant time dependent corrections, the PMC model predicts

$$G(z) \doteq \frac{\varrho_m k_B T}{N_c}\left\{ \frac{-1}{z}\left(1 - \frac{2}{M_0 c_2}\right) + \frac{2\mu(z)}{M_0^2 c_2} + \frac{-w}{zM_0}\left(\frac{-z\Sigma'(z)}{M_0}\right)^{1/(1+2\nu)}\right\}, \quad \text{for } 1/\tau^{RR} \ll z \ll 1/\tau_c, \tag{49a}$$

where

$$w = \frac{2N_c}{c_2(1+2\nu)\sin\left(\frac{\pi}{1+2\nu}\right)}.$$

The power law tails of the memory functions, Eqs. (42) and (45), introduce frequency dependent relaxation in the plateau region. Physically, this corresponds to the early stage of the disentanglement process associated with the anomalous segmental diffusion and small scale polymer shape fluctuations. Fractal power laws can be observed in the loss, $G''(\omega)$, and the storage, $G'(\omega)$, part of the shear modulus. The contributions from $\Sigma'(z)$ in Eq. (49a) can be viewed as the low frequency wing of the glassy, or microscopic, dynamics which peaks at higher frequencies. (This already indicates that local modes, discussed in the next section, will hide this contribution.) The dynamic part of the internal memory function, i.e., $\mu(z)$, describes the high frequency wing of the final entanglement decay centered around $\omega\tau_D \approx 1$

$$G'(\omega) - G_c \propto G''(\omega) \propto \begin{cases} \dfrac{1}{N^{2-d\nu}}\left\{ \pm \dfrac{\omega^{-\frac{(2-d\nu)(\nu(d+2)-1)}{(1+2\nu)^2}}}{N^{2-d\nu}} + c\dfrac{\omega^{\frac{(\nu(d+2)-1)^2}{(1+2\nu)^3}}}{N^{\frac{2-d\nu}{1+2\nu}}}\right\}, & 1/\tau^{R} \ll \omega \ll 1/\tau_c, \\ \dfrac{1}{N^{4-2d\nu}}\left\{ \pm \dfrac{\omega^{-\frac{2-d\nu}{1+2\nu}}}{N^{\frac{(2-d\nu)^2}{1+2\nu}}}\right\}, & 1/\tau^{RR} \ll \omega \ll 1/\tau^{R}, \end{cases} \tag{49b}$$

where $\pm$ denotes the two cases, G'' and G', respectively. For Gaussian chains in three dimensions, $\nu = 1/2$ and $d = 3$, the power laws, $G''(\omega) \propto \omega^{-3/16}/N + c\,\omega^{9/32}/N^{3/4}$ in the first frequency window, and $G''(\omega) \propto \omega^{-1/4}/N^{9/8}$ in the second region had been found previously.[30] In the limit of $d_F = d = 3$, lower dynamical amplitudes and somewhat different exponents are found, $G''(\omega) \propto \omega^{-6/25}/N^2 + c\,\omega^{12/125}/N^{8/5}$, and $G''(\omega) \propto \omega^{-3/5}/N^{13/5}$ in the two regions. It can be noted that the high frequency wing, $1/\tau^{R} \ll \omega \ll 1/\tau_c$, of the entanglement peak in the shear loss modulus follows a power law with an exponent,

$$x = \frac{(2-d\nu)(\nu(d+2)-1)}{(1+2\nu)^2},$$

which lies in the range 0.2 ± 0.05 for $1/3 \leqslant \nu \leqslant 1/2$ and $d = 3$. In time space this predicts that the initial decay below the plateau modulus is described by the fractal law: $G(\tau_c \ll t \ll \tau^{R}) - G_c \propto -t^{x}$. The decay of $G(t)$ onto the plateau or the range in G' and G'' where $G' \propto G'' \propto \omega^{\delta}$ and $\delta > 0$ is driven by the local modes, $\lambda > \pi/N_c$, which will be discussed in the next section.

As all internal modes which contribute to the shear stress relax for times larger than τ^{RR} with a uniform rate, Eq. (46b), the shear modulus simplifies to an exponential process

$$G(t) = \frac{\varrho_m k_B T}{N_c} e^{-(t/\tau_D)} \quad \text{for } t \gg \tau^{RR}. \tag{49c}$$

The shear viscosity in the large-N-limit, neglecting corrections from shorter times simply follows from this

$$\eta = G_c \tau_D = \varrho_m k_B T \frac{\tau_D}{N_c} \propto \frac{\varrho_m g_d^2}{N_c} N^{5-2\nu(d-1)}. \tag{49d}$$

Since the cross-over degree of polymerization, N_c, found in the RR model, Eq. (30), does not depend on N, the viscosity scales with degree of polymerization in the same way as the terminal relaxation time, τ_D. The Stokes-Einstein ratio normalized by the size of the molecule, $D\eta/R_g^2$, can now easily be calculated from Eq. (39), as viscosity and final relaxation time differ by a factor of plateau modulus only. This ratio, $D\eta/R_g^2$, has been included in Fig. 4 and its scaling with equilibrium parameters follows from the one of the plateau modulus, G_c. The dependence of the entanglement degree of polymerization, N_c in Eqs. (30) and (31), and of the final

relaxation time, τ_D of Eqs. (37), on structural equilibrium parameters determine the scaling of the viscosity with density in the theta and good solvent cases. For ideal Gaussian coils in $d=3$ dimensions the results $\eta \propto N^3 \varrho_m^5$ and $\eta \propto N^3 \varrho_m^{7/2}$ had been reported for theta and good solvent, respectively.[34] If the dimensions are $d_F = 1/\nu = d = 3$ then $\eta \propto N^{11/3}$ and exponential density dependence for theta solvents, and $\eta \propto N^{11/3} \varrho_m^{41/9}$ for good solvents results.

For intermediate times, the radius of gyration fluctuations, $P(t)$ from Eq. (22), are also arrested at the initial value, $P(t=0) = (c_2)/(2\pi\nu)\,\lambda_c^{-2\nu} \propto R_g^2$

$$P(z)/P(t=0) = \frac{-1}{z} - \frac{-1}{z}\,\frac{(-z\Sigma'(z))^{-\frac{2\nu}{1+2\nu}}}{P(t=0)M_0^{\frac{1}{1+2\nu}}}, \quad \text{for}$$

$$1/\tau^{\mathrm{RR}} \ll z \ll 1/\tau_c\,. \tag{50a}$$

In contrast with the stress relaxation, the dominance of the lowest lying internal modes in $P(t)$ interestingly leads to the memory function Σ' dominating the slow initial relaxation of $P(t)$ away from its initial plateau. The high frequency wing of the main relaxation peak in $P(t)$ at τ_D follows from Eqs. (42) and (44)

$$P''_{(\omega)}/P(t=0) \propto \begin{cases} \omega^{-\frac{2\nu(\nu(d+2)-1)^2}{(1+2\nu)^3}} N^{-\left(2\nu+\frac{2-d\nu}{1+2\nu}\right)} & 1/\tau^{\mathrm{R}} \ll \omega \ll 1/\tau_c\,, \\ \omega^{-\frac{2\nu(\nu(d+2)-1)}{(1+2\nu)^2}} N^{-\left(2\nu+\frac{2-d\nu}{1+2\nu}\left(1+\frac{2\nu(\nu(d+2)-1)}{1+2\nu}\right)\right)} & 1/\tau^{\mathrm{RR}} \ll \omega \ll 1/\tau^{\mathrm{R}}. \end{cases} \tag{50b}$$

The exponents for the power laws describing Gaussian chains in $d=3$, $P''_{(\omega)}/P(t=0) \propto \omega^{-9/32} N^{-5/4}$ and $P''_{(\omega)}/P(t=0) \propto \omega - 3/8 \mathrm{N} - 23/16$, astonishingly are not too far from the exponents exhibited by the shear modulus, although their origin within the theory is totally different. This accidental similarity does not hold for $d_F = d = 3$, where one finds $P''_{(\omega)}/P(t=0) \propto \omega^{-8/125} N^{-19/15}$ and $P''_{(\omega)}/P(t=0) \propto \omega^{-4/25} N^{-107/75}$ in the first and second time window, respectively. The predicted power laws are expected to be relevant to dielectric loss measurements. The final relaxation of $P(t)$, of course, is influenced by the lowest eigenmodes of the molecule. Extending the mode-independent exponential long time law, Eq. (46b), down to global modes, $\lambda \approx \lambda_c \approx \pi/N$, one misses prefactors which are slowly varying compared to the dominant exponential relaxation

$$P(t) \approx P(t=0) e^{-(t/2\tau_D)} \quad \text{for } t \gg \tau^{\mathrm{RR}}. \tag{50c}$$

The non-exponential dynamical behavior of $P(t)$ in the intermediate time window results from the uniform drag function, Σ', which has a short, microscopic characteristic frequency. Therefore, the crossover to the exponential relaxation in Eq. (50c) is expected to be observable more easily than the corresponding crossover in $G(t)$, Eq. (49c), which requires times long compared to the characteristic time of $M(t)$, which is of the order of τ^{RR}.

D. Finite *N* corrections and model calculations

In the previous sections, the limiting results of the PMC model for large degrees of polymerization, N, were presented. Experimentally, ratios of $N/N_c \lesssim 300$ have been achieved for entangled linear chain polymer liquids, with values of $N/N_c \lesssim 100$ a common upper bound.[6] In attempting to compare the results of the previous section to experiments, one has to take into account the possibility for significant finite N-corrections. Also, it is expected that the entanglement effects captured in the PMC model should not affect the very local and fast dynamics. Therefore, no results for times shorter than the crossover time τ_c have been reported in the previous sections. These questions have been addressed recently by switching off the PMC-memory functions for high, local modes.[31,32] These studies, where $m^\lambda(z) \to \Theta(\pi/N'_c - \lambda) m^\lambda(z)$ is one simple choice of an abrupt cut-off, were performed numerically and lead to results which compare favorably with shear stress and other measurements in chain polymer solutions and melts.[31,32,76] In the present work, we want to incorporate the most important qualitative corrections into the analytic large N results in a simple, semi-quantitative way. We use the above cut-off procedure, and choose $N'_c = N_c$ for simplicity, describing the high λ modes according to the bare Rouse model, $C^\lambda(t) = e^{-\lambda^{1+2\nu} t/c_2}$ for $\lambda > (\pi/N_c)$.

The center-of-mass motion is not affected by this cutoff procedure. The translational diffusion coefficient for small N will be close to its Rouse value, $D^{\mathrm{R}} = 1/N$, not the asymptotic prediction of Eq. (38). Equation (17a) suggests a sensible naive interpolation:

$$\frac{D^{\mathrm{R}}}{D} = 1 + \left(\frac{N}{N_D}\right)^{4-2d\nu}, \tag{51}$$

where N_D is defined from Eq. (38). Of course, finite N corrections which may be important in the crossover regime from Rouse to strongly entangled behavior are ignored by this formula. The value of N_D depends on the exact numerical value of the ψ'-coupling parameter of the PMC model, which, as we argued in Section III, the coarse-grained thread-PRISM calculation cannot reproduce. The unknown numerical prefactor in ψ', which was called B in Section III, scales the thread ψ' for Gaussian chains to the previously reported values of string-PRISM calculations;[33] $B=7$ is used. This gives values for N_D roughly equal to N_c for Gaussian chains and fixes the comparison for different fractal dimensions. Results for N_D are included in Fig. 3. More dense fractal objects follow the Rouse-like behavior in the

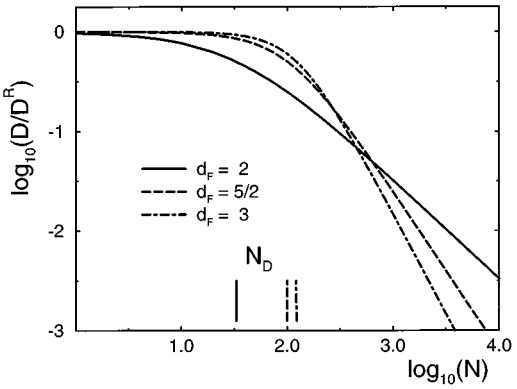

FIG. 5. Logarithmic plot of the reduced diffusion coefficients from Eq. (51) versus degree of polymerization for different fractal dimensions. The vertical lines mark the crossover degrees of polymerization, N_D, from Fig. 3.

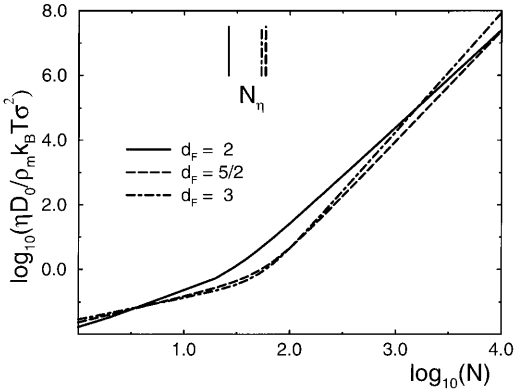

FIG. 6. Logarithmic plot of the reduced shear viscosities from Eq. (53e) versus degree of polymerization for different fractal dimensions. The vertical lines mark the crossover degrees of polymerization, N_η, from Fig. 3.

diffusion coefficient up to higher degrees of polymerization than Gaussian chains. This results from the faster decay of the vertices in the PMC-memory functions, i.e., $\Sigma(z)$ in this case, in the self-similar region of the collective structure of the macromolecule, $\omega_q \propto q^{-d_F}$, for $qR_g \gg 1$. This effect in the prefactor can even cancel the stronger N-scaling of the entanglement friction found for more dense fractal macromolecules. The comparison in Fig. 5 of diffusion coefficients for different fractal dimensions plotted versus degree of polymerization shows that in the typical, experimentally accessible range ($N/N_D < 100$) differences between the curves of less than half a decade are obtained. Only for N's higher than order $N \approx 10^3$ ($N/N_D \approx 300$ for ideal Gaussian chains), do the large N-scaling powers dominate over the prefactors.

Whereas the local modes do not affect the center-of-mass motion, the averaged mean squared displacement, $\phi(t)$, is dominated by them at short times

$$\Delta\phi(z) = \frac{-2}{z}\int_{\pi/N_c}^{\infty}\frac{d\lambda}{\pi}\frac{1}{\Gamma^{\lambda} - iz}, \tag{52a}$$

which leads to the appropriate unentangled Rouse-like motion at short times

$$\Delta\phi(t) \propto \begin{cases} t^{\frac{2\nu}{1+2\nu}}, & t \ll \tau_c, \\ N_c^{2\nu}, & t \gg \tau_c. \end{cases} \tag{52b}$$

The dynamics of the local modes dominates over the PMC result,

$$\phi(t) \propto t^{\frac{2\nu}{1+2\nu}} \Big/ N^{\frac{2-d\nu}{1+2\nu}},$$

for $t \ll \tau_c$ and completes the results for $\phi(t)$ in Eq. (47). As the results for $\phi(t)$ for longer times are dominated by the broad range of internal modes, small corrections because of the cut-off are found there. This also holds for the radius of gyration correlator, $P(t)$, since the static amplitude factors imply that it is dominated by the long range modes ($\lambda \ll \pi/N_e$) of the macromolecule.

The shear stress, $G(t)$, is affected by the local modes more strongly. All internal modes contribute equally to Eq. (21), and consequently the corrections of the local modes cannot be neglected. The contribution of the local modes, $\Delta G(t)$, has to be added to the PMC-shear modulus and again dominates for short times or high frequencies

$$\Delta G(t) = \varrho_m k_B T \int_{\pi/N_c}^{\infty}\frac{d\lambda}{\pi} e^{-2\lambda^{1+2\nu} t/c_2}, \tag{53a}$$

$$\Delta G(z) \propto \varrho_m k_B T \begin{cases} (-iz)^{-\frac{2\nu}{1+2\nu}} & z\tau_c \gg 1, \\ i\tau_c^{\frac{2\nu}{1+2\nu}} & z\tau_c \ll 1. \end{cases} \tag{53b}$$

The unentangled local modes give rise to the low frequency wing of the glassy or segmental relaxation peak in the shear modulus. The crossover from this N-independent spectrum to the high frequency tail of the entanglement relaxation process gives rise to a minimum in the loss shear modulus. A simple additive interpolation formula is given by

$$-zG(z) \propto G_c \times \left\{ 1 - \frac{(2c_2c_7)\tau_c^{\left(\frac{2-d\nu}{1+2\nu}\right)^2}}{c_4^2\psi'} \frac{(-iz)^{-\frac{(2-d\nu)(\nu(d+2)-1)}{(1+2\nu)^2}}}{N^{4-2d\nu}} + \Gamma\left(\frac{2\nu}{1+2\nu}\right)(-iz\tau_c)^{\frac{1}{1+2\nu}} \right\} \quad \text{for } z\tau^{\mathrm{R}} \gg 1. \tag{53c}$$

Only for large N, the second power law in the frequency range $1/\tau^{\mathrm{R}} \ll \omega \ll \tau_c$, see Eq. (49b), will be observable as well. For smaller frequencies, the low frequency wing of the minimum crosses over to the power law in the second time window of Eq. (49b). Figure 7 shows the storage and loss parts of the shear modulus for fractal dimensions $d_F = 1/\nu = 2$ and $d_F = d = 3$. With increasing degree of polymerization the storage modulus arrests more completely at its plateau value, whereas the minimum in the loss modulus becomes deeper and shifts to lower frequencies. The minimum position and loss value, $G''_{\min} = G''(\omega_{\min})$, exhibit the following trends:

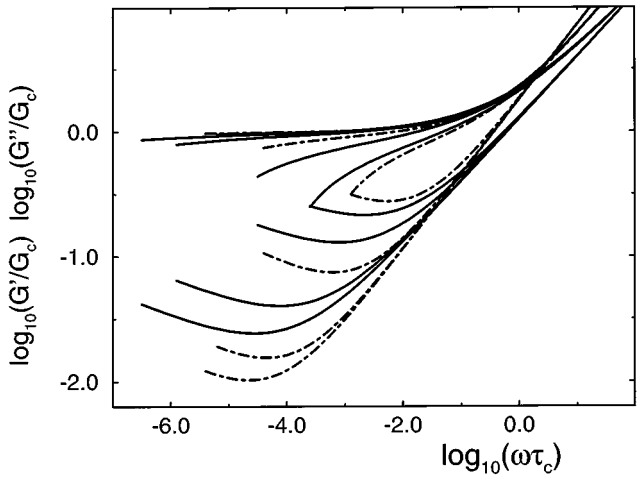

FIG. 7. Logarithmic plot of the normalized shear storage, $G'(\omega)$, and loss, $G''(\omega)$, modulus versus reduced frequency [τ_c from Eq. (30b)] as described by the interpolation formula (53c) in $d=3$ dimension. The curves are limited for low frequencies at either $\omega\tau^{\mathrm{R}}=0.1$ or $G'(\omega)=G''(\omega)$. Solid lines correspond to ideal Gaussian coils, $d_F=2$, for the degrees of polymerization $N=$ 130, 260, 1300 and 2600 (corresponding to $N/N_\eta=$ 5, 10, 50 and 100), and the chain curves correspond to $d_F=d=3$, for $N=$ 540, 1350, 4050 and 5400 ($N/N_\eta=$ 10, 25, 75 and 100).

$$\omega_{\min}\propto N^{-\frac{2(2-d\nu)(1+2\nu)^2}{(1+2\nu)+(2-d\nu)(\nu(d+2)-1)}},$$

$$\text{and}\quad G''_{\min}\propto N^{-\frac{2(2-d\nu)(1+2\nu)}{(1+2\nu)+(2-d\nu)(\nu(d+2)-1)}}. \tag{53d}$$

For ideal Gaussian coils in $d=3$ dimension this predicts $G''_{\min}\propto\omega_{\min}^{1/2}\propto N^{-8/11}$, whereas for $d_F=1/\nu=d=3$ $G''_{\min}\propto\omega_{\min}^{3/5}\propto N^{-10/7}$ follows. Consequently, the loss tangent, i.e., the ratio $\tan\delta=G''_{\min}/G'_{\min}$, scales more strongly with N for higher d_F, as follows from Eq. (53d). From the numerical prefactors in Eq. (53c) it follows, as can be seen in Fig. 7, that roughly the same ratio N/N_η in the experimentally relevant N-range is required for the different fractal dimensions in order to achieve an observation of a roughly equal entanglement plateau effect, characterized by the frequency window in which $G'(\omega)>G''(\omega)$. For ideal Gaussian chains the required N values to observe the onset of the plateau compares nicely to experimental results.[6,58] However, depends sensitively on the prefactor in Eq. (53c), which has been calculated using the coarse-grained thread-PRISM model, and reinforces the need to study the non-asymptotic correction numerically.[31,32,76] Eq. (53c) breaks down at higher frequencies, where it crosses over to the glassy peak, but also at lower frequencies, due to the terminal relaxation step. For the sake of demonstration, in Fig. 7 the window of validity of Eq. (53c) is estimated by extending the curves down to $\omega\tau^{\mathrm{R}}=0.1$ or $G'(\omega)=G''(\omega)$.

A numerical calculation of the shear modulus and the shear viscosity for intermediate N is beyond the scope of this paper. Following common practice and the idea used in Eq. (51), we use a simple interpolation between the bare Rouse result, $\eta^R=\varrho_m k_B T(c_2/4\pi\nu)\lambda_c^{-2\nu}$, where, $\lambda_c=\pi/N$ is chosen, and the result Eq. (49d) for large N

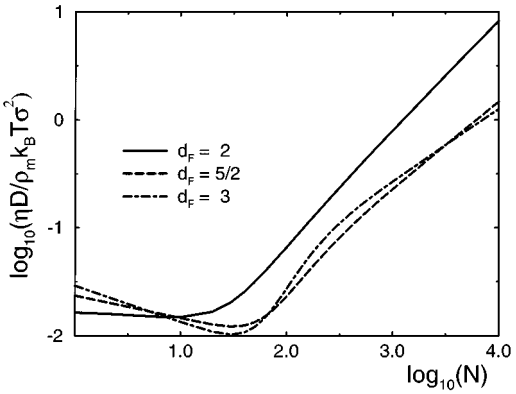

FIG. 8. Logarithmic plot of the normalized product of the diffusion coefficient and shear viscosities from Eqs. (51 and 53e) versus degree of polymerization for different fractal dimensions.

$$\frac{\eta}{\eta^{\mathrm{R}}}=1+\left(\frac{N}{N_\eta}\right)^{5-2d\nu}. \tag{53e}$$

The degree of polymerization, N_η, where the viscosity crosses over from the Rouse limit to the entangled limit is implicitly defined by Eqs. (49d) and (53e) and included in Fig. 3. The values of N_η and N_c are rather close for all fractal dimensions. As shown in Fig. 6, and also found for the diffusion coefficients, strong cancellation effects between the prefactors and the N scaling powers are obtained when comparing viscosities for different fractal dimension. Although the exponent of the scaling with N increases for increasing fractal dimension, the prefactor in Eq. (49) or (53e) largely counterbalances this leading to effectively smaller viscosities for intermediate N. Only for degrees of polymerization exceeding the range 10^3 to 10^4 ($N/N_\eta>50-300$), does the large N-scaling prevail. Again, this result is tied to the behavior of the vertices in the PMC-memory functions in the intermediate, self-similar wave vector regime.

A sensitive measure of these crossover issues is the Stokes-Einstein ratio, $D\eta$, which experimentally also has the advantage of being independent of the monomeric friction coefficient. Its asymptotic value, $D\eta\propto R_g^2$ follows from Eq. (39), and for finite N its shape depends strongly on both the numerical values of the crossover degrees of polymerization, and other finite N-corrections which are not contained in our description. Figure 8 shows that within our simplified crossover description, in the experimentally accessible range $N/N_c<100$, ideal Gaussian chains have a somewhat higher mobility than the more compact macromolecules of larger fractal dimension.

In principle, the full dynamics of Eqs. (16) to (23) can be worked out for finite degrees of polymerization, N. However, numerical implementations of the full PMC equations using realistic equilibrium static structure factors show that further finite-N corrections arise.[31,32,76] Therefore, a complete quantitative description of the intermediate N region is beyond the scope of this paper.

VI. DISCUSSION

The results of the RR and PMC models for ideal Gaussian chains, $\nu = 1/2$, in three dimensions, have been discussed previously[31,32] and will be taken as a reference point for the new results. Clearly, the major achievement of the present approach is to describe, starting from microscopic force-balance equations, how universal entanglement effects arise for polymers of different macromolecular architectures. Linear response dynamical correlation functions have been calculated. As the theory uses linear Langevin equations with non-Markovian and normal mode dependent memory functions, correlation functions linear in the segment positions provide stringent tests. Correlators of non-linear variables, like the coherent intramolecular dynamic structure factor, can also be obtained but only with extra Gaussian approximations. The approach incorporates an integral-equation description of the equilibrium structure of polymer melts (PRISM) and determines the dependence of non-equilibrium quantities, such as the shear stress plateau value, on equilibrium liquid parameters, such as fluid density and local aspect ratio. These dependences have been reported as scaling proportionalities but fully quantitative results based on the full PRISM equations can, in principle, be discussed. The osmotic pressure for the fractal polymer systems can as well be obtained from the solution of the thread PRISM equations via integrating the inverse compressibility:[62] $\Pi = k_B T \int_0^{\varrho_m} d\varrho' S_0^{-1}(\varrho')$. In theta solvents, one finds $\Pi \propto \varrho_m^{d\nu/(d\nu-1)}$, and in good solvents $\Pi \propto \varrho_m^{2d(\nu+1)/(d+2\nu d-2)}$, which reproduces the well established scaling forms for semidilute chain polymers in good ($\Pi \propto \varrho_m^{9/4}$) and theta ($\Pi \propto \varrho_m^3$) solvents in $d = 3$ dimensions.[2,33]

For several reasons, we believe the dynamical results provide new insight into the origin of entanglements within our theoretical description. First, as has been discussed for the Gaussian chain case,[27,30] pairwise excluded volume interactions and intramolecular connectivity enforce the uncrossability constraints and lead to corrections to the unentangled Rouse results. The corrections scale like the number, Z, of binary two-molecule contacts within the volume given by the size of the molecule, $Z \propto N^{2-d\nu}$. Strong entanglement effects therefore arise for fractal dimensions above a threshold,[30] $d_F = 1/\nu > d/2$. As discussed in detail in the Appendix, polymers scaling like rods, $R_g \propto N$, fall below this threshold and qualitatively different effects, like the absence of the plateau in the shear modulus, are obtained. Although the experimental[53] and simulation data[54,55] provide no fully convincing picture, this prediction of PMC apparently is incorrect; it strongly differs from the reptation/tube results.[3,83] Within the theory the lack of entanglement effects for rodlike macromolecules (or for $\nu > 2/d$ in general) can be traced back to the vanishing number of internal modes. The theory approximates the slow intermolecular, fluctuating forces by their overlap with, and the dynamics of, the self-similar spectrum of internal modes as they contribute to the single molecule structure factor. This misses special topological entanglement effects as is shown for Gaussian rods in the Appendix. However, this does not invalidate the approach to flexible polymers or to semiflexible ones, as long as the persistence length is small compared to the crossover length r_c. For $\nu < 2/d$ it appears unlikely that the effects of low lying modes, i.e., rotation, which dominate the rigid rod entanglements, will be important compared to the slowing down of the broad band of internal modes.

Second, as is intuitively expected, entanglements are effective only if different macromolecules can interpenetrate. This becomes more difficult for objects with a fractal dimension approaching the dimension of the space they are embedded in. In the present approach this is predicted by the increase in the packing fraction, ϕ, required to obtain similar melt structures, i.e., identical (normalized) bulk compressibilities in our case. Accompanying the change in ϕ is a decrease in the contact value of the pair correlation function, which is a local measure of the binary collisions.[27,62] Consequently, entanglement effects are predicted to be present even in the extreme case of equal fractal and spatial dimensions. However, the necessary densities to force interpenetration turn out to be so high (see Fig. 1) that experimental detection appears impossible. This agrees with the experimental observations that rather dense fractal micro-networks,[17] $d_F \approx d = 3$, and computer simulations of Gaussian chains melts in two dimensions[56] appear to show no entanglement effects. The connection of the theoretical results to experiments on melts of non-interpenetrating, non-fractal micro-gels,[16] which exhibit entanglement effects strikingly similar to linear chains, is unclear at present. As briefly mentioned in Section V B, for swollen Gaussian polymers with fractal dimension $d_F = \frac{4}{3}$ in two dimensions the theory predicts that the diffusion coefficient scales like $D \propto N^{-2}$. This exponent agrees well with a recent simulation of linear, self-avoiding walk polymers in a two dimensional system of obstacles in the limit of a high density of obstacles.[74] It should be noted that here the seeming agreement with the reptation exponent is misleading as the correct reptation prediction[30] would be $D \propto R_g^2/N^3 \propto N^{-3/2}$.

Third, transport coefficients, like the diffusion coefficient or the shear viscosity, are predicted to scale with molecular weight with exponents varying in between -2 and -3, and 3 to 11/3, respectively, for fractal dimensions of $d_F = 2$ to $d_F = 3$ in three dimensions. The prefactors, related to microscopic structural properties such as ψ and ψ', determine the crossover degrees of polymerization, N_D and N_η. They, however, show an opposite trend. This cancelation, or compensation, effect is physically significant and directly results from the self similar range in the intra-molecular structure where $\omega_q \propto q^{-d_F}$. Calculated diffusion coefficients or viscosities for different d_F are rather close for molecular weights which lie in the range of present day experiments. This prediction agrees qualitatively with the comparison of viscosity data for polystyrene linear chains and rings, where similar magnitudes but slightly higher exponents for ring macromolecules are reported.[11] The product $D\eta$ is a sensitive parameter for the dynamics of different fractal macromolecular melts. In the crossover N range consistently larger values of $D\eta$ for ideal Gaussian chains are obtained than for

the macromolecules characterized by larger fractal dimensions.

The ratio $D\tau_D/R_g^2$ asymptotically becomes N- and chemistry-independent, and only depends weakly on spatial and fractal dimensions. This demonstrates that an underlying diffusive transport process dominates the relaxation of the entanglement friction in the PMC model, in qualitative accord with the reptation/tube model. The generality of the microscopic description based on ensemble-averaged correlation and memory functions, however, precludes easy visualization of the macromolecular motion at the N-body, trajectory level addressed by the phenomenological tube model approach.

The hallmark of entanglements, a nearly elastic response in an intermediate time window but continuous, anomalous translational diffusion, is obtained in the theory for different fractal macromolecules if they interpenetrate. It arises from the arrest of internal modes which lie in the self similar regime of the intra-molecular structure. The resulting plateau value of the shear modulus varies little with fractal dimension. The loss tangent, tan $\delta = G''_{\min}/G'(\omega_{\min})$, however, depends more strongly on degree of polymerization for denser (fractal) macromolecules. These trends are also present when comparing the experimental results of the denser, non-fractal micro-gels (tentatively modeled with a fractal dimension $d_F \approx 3$) and their linear chain analogs.[16,58,59] Fractal power law relaxations are superimposed on the arrested contribution, the effective temporal exponents of which are tightly connected to the equilibrium fractal structure. The observation of rather universal shear spectra in this intermediate frequency window for linear chains[58,59] and cyclic polymers[10] supports this physical picture of entanglement formation and the early and intermediate stages of the disentanglement. Unfortunately, the experiments on polymer rings do not extend to high enough molecular weights to clearly detect the difference in the shear spectra expected from our results and the conjecture $d_F = 5/2$ for rings in melts.[46,47] Compared to the reptation prediction of an exponent 1/2 for the high frequency wing of the shear loss modulus ($G'' \propto \omega^{-1/2}$ for $\omega\tau_D \gg 1$), the PMC predictions of exponents of approximatively 0.2 to 0.25 for ideal chains in $d = 3$ dimensions are in much closer agreement with the experiments.[10,16,58,59,77] As discussed in Refs. 31 and 32, and work in progress[76] shows, the shape of the shear modulus spectra, $G'(\omega)$ and $G''(\omega)$, of linear chain melts can be extremely well described by the present theory, especially when finite N corrections are numerically taken into account.

ACKNOWLEDGMENTS

Stimulating discussions and correspondence with Professor M. Antonietti are gratefully acknowledged. We thank Dr. E.F. David for providing the programs used to solve the full PRISM equations numerically. Partial financial support by the Deutsche Forschung Gemeinschaft under Grant No. Fu 309/1-1, and the United States National Science Foundation MRSEC program via Grant Number NSF-DMR-89-20538, are acknowledged.

APPENDIX

The model of Gaussian fractal rods, $\omega_{\alpha\beta}(q) = \exp\{(-q^2/2d)(\alpha-\beta)^2\}$ and $R_g \propto N$, shares with real rods that the only dynamical modes possible are translation and rotation.[65] This simplification can be exploited in order to study the rotational-translational coupling of the RR and PMC dynamics. The matrix of the intra-molecular elastic forces possesses one finite eigenvalue, the rotational relaxation time, $\tau_0^{\mathrm{Rot}} = N(N^2-1)/12$ (dimensionless variables from Section III B), with eigenvector

$$V_{\mathrm{Rot}}^T = \left(-\frac{N-1}{2}, -\frac{N-3}{2}, \ldots, \frac{N-1}{2} \right) / \sqrt{\tau_0^{\mathrm{Rot}}}.$$

From Eq. (13b) one obtains its form[65]

$$\overline{\Gamma}^{-1} = \frac{1}{\varepsilon} P_{\mathrm{CM}} + \tau_0^{\mathrm{Rot}} V_{\mathrm{Rot}} V_{\mathrm{Rot}}^T. \tag{A1}$$

In the case of interacting Gaussian rods the dynamical matrix of segment positions results from center-of-mass motion, $\Phi(t)$, rotation, $\varphi_{\mathrm{Rot}}(t)$, and their cross-coupling, $\Delta(t)$. In the PMC model the dynamics of translation and rotation is described by a 2×2 matrix system of coupled equations, which are obtained when projecting Eq. (1) onto the appropriate directions. In the case of a single freely moving Gaussian rod, the results are well known[65] $\Phi(t) = 2t/N$, $\varphi(t) = e^{-t/\tau_0^{\mathrm{Rot}}}$ and $\Delta(t) = 0$. The dynamic structure factor is obtained easily due to the Gaussian nature of the intra-molecular distribution

$$\omega^{(\mathrm{R})}(q,t) = \frac{1}{N} \sum_{\alpha,\beta=1}^{N} \omega_{\alpha\beta}(q) \exp\left\{ -\frac{q^2}{2d} [\Phi(t) + \tau_0^{\mathrm{Rot}} V_\alpha^{\mathrm{Rot}} V_\beta^{\mathrm{Rot}} (\varphi(t) - 1)] \right\} \tag{A2}$$

$$\approx \frac{N}{(1 + c_1 q^2 N^2)^{1/2}} e^{-\frac{q^2 t}{dN}} \quad \text{for Rouse case,}$$

$$\text{where } c_1 = \frac{1}{2d\pi}. \tag{A3}$$

The final approximation in Eq. (A3) agrees qualitatively with the exact result for the non-interacting case in all limits. Due to the missing internal modes, the dynamics structure factor relaxes diffusively for all wave vectors. The Rouse dynamic structure factor enters the RR-friction function, $\Lambda(z)$ in Eq. (2a), which is given by

$$\Lambda(z) = \tilde{\psi} \int_0^{q_c} dk k^{d+1} S_k \omega_k \frac{-1}{z + i(k^2/dN)}, \tag{A4}$$

where

$$\tilde{\psi} = \psi / S_0.$$

The static structure factor will be discussed below.

In the memory functions of the PMC model the scalar products of the translational and rotational eigenvectors with the inverse intra-molecular structure factors are needed, e.g., $V_{\mathrm{CM}}^T \omega^{-1} V_{\mathrm{CM}}$. Note that the density of states, Eq. (24b), can-

not be used for these projections as it correctly describes the distribution of the eigenvalues only. Here, however, the exact projections on the eigenvectors of the two lowest lying states are needed. Fortunately, for Toeplitz matrices the problem of calculating the matrix inverse simplifies considerably.[78–80] The inverse of a symmetric and real, N-dimensional Toeplitz matrix, $\omega_{(\alpha-\beta)}$, has the following structure[78]

$$\omega^{-1}=\frac{1}{x_1}(L_1L_1^T-L_2L_2^T), \tag{A5a}$$

where the matrices L_1 and L_2 are lower triangular matrices determined from N numbers, x_α with $\alpha=1,\ldots,N$

$$L^1_{\alpha\beta}=x_{1+\alpha-\beta} \quad \text{for} \quad \alpha\geqslant\beta,$$
$$L^2_{\alpha\beta}=x_{N+1-(\alpha-\beta)} \quad \text{for} \quad \alpha>\beta, \quad L^1_{\alpha\beta}=L^2_{\alpha\beta}=0 \ \text{ else.} \tag{A5b}$$

The numbers x_α are the elements of the first row of the inverse matrix and can be found from Yule-Walker equations[79,80]

$$\sum_{\beta=1}^{N}\omega_{(\alpha-\beta)}x_\beta=\delta_{\alpha,1} \quad \text{for} \quad \alpha=1,\ldots,N. \tag{A5c}$$

One can use the Levinson algorithm[79] in order to prove that the inverse of the Gaussian rod intramolecular structure matrix, $\omega_{\alpha\beta}(q)=f^{(\alpha-\beta)^2}$, can be obtained from[81]

$$x_\alpha=(-f)^{\alpha-1}\left(\prod_{\beta=1}^{N}(1-f^{2\beta})\right)^{-1}\prod_{\beta=\alpha}^{N-1}\left(\frac{1-f^{2\beta}}{1-f^{2(N-\beta)}}\right)$$
$$\text{for} \quad 1\leqslant\alpha\leqslant N, \tag{A6}$$

The ill-conditioned nature of the inverse appears in the small q asymptotes, $x_\alpha\sim q^{-(N-1)}$ for $q\to 0$. The ill-behavior is caused by the singular nature of the intra-molecular elastic matrix, Γ, and a direct consequence of the existence of only two degrees of freedom in the rod molecule. It necessitates the use of the exact inverse in order to cancel the contributions from the internal modes, $p\geqslant 2$, which acquire infinite spring constants in the limit $q\to 0$.

The cross-coupling vanishes in the asymptotic limits, $V^T_{\mathrm{Rot}}\omega^{-1}V_{\mathrm{CM}}\to 0$ for $qR_g\to 0$ and $qR_g\to\infty$. Therefore, the memory function coupling translational and rotational dynamics can be neglected to a good approximation and the dynamics decouple. This leads to Eq. (17a) for the center-of-mass motion and for the rotational correlator one obtains

$$\varphi(z)=-\left(z+\frac{i/\tau_0^{\mathrm{Rot}}}{1-iM(z)}\right)^{-1}.$$

The memory functions appropriate for entangled rods follow with a simple interpolation of the asymptotes and are influenced by the melt structure as discussed below.

$$\Sigma(z)=\tilde{\psi}'\int_0^{q_c}dk k^{d+1}S_k\omega_k\frac{-1}{z+\dfrac{i(k^2/dN)}{1-i\Lambda(z)}}, \tag{A7a}$$

$$\text{where } \tilde{\psi}'=\psi'/S_0,$$

$$M(z)=\tilde{\psi}'\int_0^{q_c}dk k^{d-1}S_k\omega_k\left(\frac{1}{c_1N^2}+k^2\right)\frac{-1}{z+\dfrac{i(k^2/dN)}{1-i\Lambda(z)}}. \tag{A7b}$$

Another physically more intuitive way to obtain Eqs. (A7) considers from the start only the two degrees of freedom, translation and rotation. The mode coupling approximations invoked in the PMC description are repeated but projections only onto the translational and rotational components of the intra-molecular density fluctuations are carried out; i.e., $\varrho_q^{\mathrm{CM}}\propto\Sigma_\alpha V_\alpha^{\mathrm{CM}}e^{i\vec{q}\vec{R}_\alpha}$ and $\varrho_q^{\mathrm{Rot}}\propto\Sigma_\alpha V_\alpha^{\mathrm{Rot}}e^{i\vec{q}\vec{R}_\alpha}$. Qualitatively identical results to Eq. (A7) are obtained; again rotational-translational coupling is found to be negligible. The above approach, however, more clearly shows the connections to the other fractal models.

Few binary contacts result from the very open intra-molecular structure of Gaussian rods, $\omega_q\propto 1/q$ for $qR_g\gg 1$. Consequently, the RR and PMC-memory functions are dominated by the molecular weight independent local static structure, simplistically described by an wave vector upper cut-off q_c. No intermediate time windows of anomalous dynamics open up, where either translation or rotation are effectively frozen. The characteristic times of the memory functions are easily found to be $\tau\sim N/q_c^2$. Except for minor, rapidly decaying long time tails, the effects of the RR and PMC memory functions is to provide an extra, molecular weight and density dependent contribution to the friction coefficient affecting diffusion coefficient and rotational time in the same way

$$\frac{\tau^{\mathrm{Rot}}}{\tau_0^{\mathrm{Rot}}}=\frac{D_0}{D}=1+\varrho L^2\sigma(c_0^2/\sigma^6)(a+\varrho L^2\sigma g_d^2\tilde{a}). \tag{A8}$$

The spatial dimension is restricted to $d=3$; logarithmic dependences on the degree of polymerization result in $d=2$. The numerical constants, a and $\tilde{a}$, are of order unity. Equation (A8) is expressed using the standard physical parameters of rod length, $L=N\sigma$, and rod concentration, $\varrho=\varrho_m/N$.

The intermolecular equilibrium structure enters Eq. (A8) via the contact value of the pair correlation function, g_d, and the $q=0$ value of the repulsive direct correlation function, c_0. It can easily be argued that both parameters are density and molecular weight independent, since the relevant density range is limited by the occurrence of the isotropic to nematic phase transition of rod molecules[3] at a reduced density of order unity. $\varrho L^2\sigma<1$. From the PRISM equations (26) and assuming a finite direct correlation function, one can see that for such low densities the collective structure factor differs little from the intra-molecular one, $S_q\approx\omega_q$. This aspect was already used in Eqs. (A4) and (A7). Using a cut-off in the thread-PRISM equations (27) shows that c_0 is of order unity for rods described by the fractal intra-molecular structure of Eq. (A3). Similarly, the contact value g_d is found to be small, but of order unity. Numerical solutions to the full PRISM equations (26) for finite diameter rods are available.[82] For the small densities of interest, $\varrho<1$, the di-

rect correlation function can be estimated from the contact value, $c_0 \approx 4\pi/3 g_d D^3$, which can directly be determined in simulations.[54,55]

A feature of this result in disagreement with simulations of rigid rod molecules is that translational and rotational diffusion are affected in equally strong ways. Simulations find that the relative decrease of the rotational diffusion coefficient by a little more than a decade exceeds the accompanying relative decrease of the total translational diffusion coefficient by a factor of roughly three.[54,55] The dependence in Eq. (A8) on the dimensionless density, $\varrho^* = \varrho L^2 \sigma$, demonstrates that excluded volume interactions lead to the slowing down. Purely topological constraints,[83–85] which hinder the motion of infinitely thin rods, lead to anisotropic motion and to the appearance of the reduced density, $\varrho^*_{\mathrm{top}} = \varrho L^3$. Clearly, our considerations of isotropic dynamics apply to angle-averaged quantities only. The isotropic averaging in our approach appears to destroy the anisotropic, topological constraints peculiar to the limit of very thin rods, $L/\sigma \gg 1$. In contrast to the other fractal dimensions where the broad range of internal modes causes the fluctuating force correlations and the entanglement effect in the theory, this peculiarity of the rod-like macromolecules within our approach does not seem surprising. For $d_F = 1$ the PMC approach couples the forces to a small number of degrees of freedom which may well be irrelevant compared to other constraining effects. However, the latter seem negligible compared to the contributions from the broad band of internal modes, whenever they are present, i.e., for $\nu < 2/d$.

[1] J. D. Ferry, *Viscoelastic Properties of Polymers* (Wiley, New York, 1980).
[2] P. G. de Gennes, *Scaling Concepts in Polymer Physics* (Cornell University, Ithaca, 1979).
[3] M. Doi and S. F. Edwards, *The Theory of Polymer Dynamics* (Oxford University, Oxford, 1986).
[4] M. Doi, J. Polym. Sci. Polym. Lett. **19**, 265 (1981); J. Polym. Sci. Polym. Phys. Ed. **21**, 667 (1983).
[5] W. W. Grassley, Adv. Polym. Sci. **47**, 68 (1982).
[6] T. P. Lodge, N. Rotstein and S. Prager, Adv. Chem. Phys. **79**, 1 (1990).
[7] J. F. Douglas and J. B. Hubbard, Macromolecules **24**, 3163 (1991).
[8] M. F. Herman, J. Chem. Phys. **89**, 3892 (1990); Macromolecules **25**, 4925 (1992); J. Chem. Phys. **103**, 4324 (1995).
[9] A. P. Chatterjee and R. Loring, J. Chem. Phys. **103**, 4711 (1995), and references therein.
[10] J. Roovers, Macromolecules **21**, 1517 (1988).
[11] G. B. McKenna, B. J. Hofstetter, N. Hadjichristidis, L. J. Fetters, and D. J. Plazek, Macromolecules **22**, 1834 (1989).
[12] T. Masuda, Y. Ohta, and S. Onugi, Macromolecules **4**, 763 (1971).
[13] W. W. Grassley and J. Roovers, Macromolecules **12**, 959 (1984).
[14] J. Roovers, Macromolecules **17**, 1196 (1984).
[15] J. Roovers and P. M. Toporowski, Macromolecules **20**, 2300 (1987).
[16] M. Antonietti, T. Pakula, and W. Bremser, Macromolecules **28**, 4227 (1995).
[17] M. Antonietti, D. Ehlich, K. J. Fölsch, H. Sillescu, M. Schmidt, and P. Lindner, Macromolecules **22**, 2802 (1989); M. Antonietti, K. J. Fölsch, H. Sillescu, and T. Pakula, *ibid.* **22**, 2812 (1989).
[18] M. Antonietti and C. Rosenauer, Macromolecules **24**, 3434 (1991).
[19] J. Klein, Macromolecules **19**, 105 (1986).
[20] M. Rubinstein, Phys. Rev. Lett. **57**, 3023 (1986).
[21] M. E. Cates and J. M. Deutsch, J. Phys. (Les Ulis, Fr.) **47**, 2121 (1986).
[22] S.P. Obukhov, M. Rubinstein, and T. Duke, Phys. Rev. Lett. **73**, 1263 (1994).
[23] S. K. Nechaev, A. N. Semenov, and M. K. Koleva, Physica (Amsterdam) A **104**, 506 (1987).
[24] W. Hess Macromolecules **19**, 1395 (1986); **20**, 2587 (1987); **21**, 2620 (1988).
[25] V. G. Rostiashvili, Sov. Phys. JETP **70**, 563 (1990).
[26] K. Kawasaki, Mod. Phys. Lett. B **4**, 913 (1990).
[27] K. S. Schweizer, J. Chem. Phys. **91**, 5802 (1989).
[28] K. S. Schweizer, J. Chem. Phys. **91**, 5822 (1989).
[29] K. S. Schweizer, J. Non-Cryst. Solids **131-133**, 643 (1991).
[30] K. S. Schweizer, Phys. Scr. T **49**, 99 (1993).
[31] K. S. Schweizer and G. Szamel, Philos. Mag. B **71**, 783 (1995).
[32] K. S. Schweizer and G. Szamel, Trans. Theo. Stat. Phys. **24**, 947 (1995).
[33] K. S. Schweizer and G. Szamel, J. Chem. Phys. **103**, 1934 (1995).
[34] K. S. Schweizer and G. Szamel, Macromolecules **28**, 7543 (1995).
[35] U. Genz and T. A. Vilgis, J. Chem. Phys **101**, 7101 (1994).
[36] H. Tang and K. S. Schweizer, J. Chem. Phys. **105**, 779 (1996).
[37] H. Tang and K. S. Schweizer, J. Chem. Phys. **103**, 6296 (1995).
[38] U. Genz and T. A. Vilgis, J. Chem. Phys **101**, 7101 (1994).
[39] H. Tang, M. Guenza, and K. S. Schweizer (in preparation).
[40] P. C. Hohenberg and B. I. Halperin, Rev. Mod. Phys. **49**, 435 (1977).
[41] T. Nakayama, K. Yakubo, and R. L. Orbach, Rev. Mod. Phys. **66**, 381 (1994).
[42] W. Hess and R. Klein, Adv. Phys. **32**, 173 (1983).
[43] W. Götze and L. Sjögren, Rep. Prog. Phys. **55**, 241 (1992).
[44] M. E. Cates, Phys. Rev. Lett. **53**, 926 (1984); J. Phys. (Paris) **46**, 1059 (1985).
[45] M. Muthukumar, J. Chem. Phys. **83**, 3161 (1985).
[46] M. E. Cates and J. M. Deutsch, J. Phys (Paris) **47**, 2121 (1986).
[47] S. Geyler and T. Pakula, Makromol. Chem. Rapid Commun. **9**, 617 (1988); T. Pakula and S. Geyler, Macromolecules **21**, 1665 (1988); J. Skolnick, A. Kolinski, A. Sikorski, and R. Yaris, Polym. Preprints **30**, 79 (1989).
[48] M. Müller, J. P. Wittmer, and M. E. Cates, Phys. Rev. E **53**, 5063 (1996).
[49] M. Doi and N. Kuzuu, J. Polym. Sci. Lett. Ed. **18**, 775 (1980); D. Pearson and E. Helfand, Macromolecules **17**, 888 (1984); R. C. Ball and T. C. B. McLeish, Macromolecules **22**, 1911 (1989).
[50] L. J. Fetters, A. D. Kiss, D. S. Pearson, G. F. Quack, and F. J. Vitus, Macromolecules **26**, 647 (1993), and references cited therein.
[51] H. Yoshida, K. Adachi, H. Watanabe and T. Kotada, Polymer J. **11**, 863 (1989); D. Boese and F. Kremer, Polymer **31** 1831 (1990).
[52] M. Antonietti and H. Sillescu, Macromolecules **19**, 798 (1986); K. Schull K. Dai, E. J. Kramer, L. J. Fetters, M. Antonietti, and H. Sillescu, Macromolecules **24**, 505 (1991).
[53] R. Pecora, J. Polym. Sci.: Polym. Symp. **73**, 83 (1985), and references cited therein.
[54] I. Bitsanis, H. T. Davis, and M. Tirell, Macromolecules **21**, 2824 (1988).
[55] I. Bitsanis, H. T. Davis, and M. Tirell, Macromolecules **23**, 1157 (1990).
[56] I. Carmesin and K. Kremer, J. Phys. (Paris) **51**, 915 (1990).
[57] H. Yu, in *Ordering in Macromolecular Systems*, edited by A. Teramoto, M. Kobayashi, and T. Norisuje (Springer, Berlin, 1994).
[58] M. Baumgaertel, M. E. De Rosa, J. Machado, M. Masse, and H. H. Winter, Rheologica Acta **31**, 75 (1992); J. Jackson, M. E. De Rosa, and H. H. Winter, Macromolecules **27**, 2426 (1994).
[59] R. Kannaan and T. P. Lodge, Macromolecules (submitted, 1996).
[60] S. F. Tead, E. J. Kramer, G. Hadziioannou, M. Antonietti, H. Sillescu, P. Lutz, and C. Strazielle, Macromolecules **25**, 3942 (1992).
[61] Matrix indices $\alpha, \beta, \ldots$ and summations arising from matrix products are suppressed. The spatial vector character of positions and forces is not noted explicitly as only isotropic correlators obtained by d-dimensional scalar products enter the theory. Where appropriate the transpose ^{T} emphasizes the matrix structure. As an example the notation simplifies $\langle \vec{R}_\alpha \cdot \vec{R}_\beta \rangle$ to $\langle R_\alpha \cdot R_\beta \rangle$ and finally to $\langle R \cdot R^T \rangle$.
[62] J. P. Hansen and I. R. McDonald, *Theory of Simple Liquids*, 2nd ed. (Academic, London, 1986).
[63] M. E. Baur and W. H. Stockmayer, J. Chem. Phys. **43**, 4319 (1965).
[64] M. Appel, G. Fleischer, J. Kärger, F. Fujara, and I. Chang, Macromolecules **27**, 4274 (1994).
[65] M. Bixon, J. Chem. Phys. **58**, 1459 (1973); R. Zwanzig, *ibid.* **60**, 2717 (1974); M. Bixon and R. Zwanzig, *ibid.* **68**, 1896 (1978).
[66] U. Grenander and G. Szegö, *Toeplitz Forms and Their Applications* (University of California Press, Berkley, 1958).
[67] W. Feller, *An Introduction to Probability Theory and its Applications*, Vol. II, 2nd ed. (Wiley, New York, 1971).
[68] K. S. Schweizer and J. G. Curro, Adv. Polym. Sci **116**, 319 (1994).

[69] K. S. Schweizer and J. G. Curro, Phys. Rev. Lett. **58**, 246 (1987).
[70] K. S. Schweizer and J. G. Curro, Chem. Phys. **149**, 105 (1990).
[71] D. Chandler and H. C. Andersen, J. Chem. Phys. **57**, 1930 (1972).
[72] K. S. Schweizer and J. G. Curro, Adv. Chem. Phys. **98** (1996).
[73] K. Kremer and G. S. Grest, J. Chem. Phys. **92**, 5057 (1990).
[74] G. W. Slater and S. Y. Wu, Phys. Rev. Lett. **75**, 164 (1995).
[75] We follow standard practice in the polymer literature (Refs. 1 and 3) in defining the storage and loss parts of a modulus or memory function by $-M'(\omega)+iM''(\omega)=\omega M(z=\omega+i\epsilon)$.
[76] G. Szamel and K. S. Schweizer, J. Chem. Phys. (to be submitted).
[77] K. Adachi and T. Kotaka, Macromolecules **18**, 466 (1985); Y. Imanishi, K. Adachi and T. Kotaka, J. Chem. Phys. **89**, 7585 (1988); K. Adachi, H. Yoshida, F. Fukui, and T. Kotaka, Macromolecules **23**, 3138 (1990).
[78] I. C. Gohberg and A. A. Semencul, Mat. Issled **2**, 201 (1972) (in Russian).
[79] N. Levinson, J. Math. Phys. **25**, 261 (1947).
[80] T. Kailath, A. Vieira, and M. Morf, SIAM Rev. **20**, 106 (1978).
[81] B. B. Kimia and S. W. Zucker, Opt. Engin. **32**, 166 (1993), where $\Pi_{\beta=N}^{N-1}(\cdots):=1$.
[82] E. F. David (private communication).
[83] M. Doi, J. Phys. **36**, 607 (1975).
[84] M. Fixman, Phys. Rev. Lett. **54**, 337 (1985); **55**, 2429 (1985).
[85] G. Szamel, Phys. Rev. Lett. **70**, 3744 (1993); G. Szamel and K. S. Schweizer, J. Chem. Phys. **100**, 3127 (1994).